Supplementary Information (SI) for Nanoscale.
This journal is © The Royal Society of Chemistry 2025

Supplementary Information

Interstitial TM–P Pairing in P_3-Coordinated Wide-Gap Quantum Dots: Spin-Selective Insulating States and Enhanced Hyperpolarizability

Saraf Mohaimen Chowdhury[a,c], Ishmam Hossain[b,c], Mahdy Rahman Chowdhury[b,d*]

[a]Department of Electrical and Electronic Engineering, Port City International University, Chattogram-4202, Bangladesh;

[b]Department of Electrical and Computer Engineering, North South University, Dhaka, Bangladesh;

[c]Mahdy Research Academy, Dhaka, Bangladesh;

[d]NSU Center of Quantum Computing, Block B, Bashundhara R/A, Dhaka-1229, Bangladesh

Contents

1 Computational Methods

The electronic, magnetic, and nonlinear optical properties of the considered QDs are investigated with DFT computation techniques and carried out in the Gaussian 09W program [1]. The calculations were made using the range-separated hybrid LC-ωPBE exchange functional [2, 3] and the effective core potential LANL2DZ basis set [4]. To accurately characterize the localization or delocalization of spin densities, we require such theories that can capture effects of electron correlation and long-range exact exchange while reduces the self-interaction errors [5–7]. For a configuration with fully-filled d^{10} shell, the d-orbitals are localized and contracted, and for system like metal-chalcogenide the majority orbital contributions comes from s and p. Therefore, unlike the configurations with partially-filled d-orbitals (like Transition-metal Dichalcogenides), such systems experience less on-site Coulomb repulsion (strong correlation) but realize more delocalization error (i. e., self-interaction errors). Standard global hybrid exchange–correlation functional cannot completely cancel this self-repulsion of electrons because they include only a small, distance-independent fraction of Hartree–Fock exchange (exact exchange), which results in an insufficient (decays exponentially instead of as –1/r) asymptotic potential [8]. Range-separated hybrid functionals overcome this limitation by incorporating exact exchange in the long-range regime, where self-interaction error is a major factor, thereby providing a more accurate description of orbital localization and electronic level alignment [9, 10]. The present configurations were optimized using several range-separated hybrid functionals, and the LC-ωPBE functional provided the most smooth SCF convergence and consistent physical parameters, while other functionals either failed to converge or showed less stable results.

The magnetic ordering is specified by performing geometry optimization on the molecular structure with time-independent self-consistent field SCF calculation at different magnetic states, such as closed-shell approach (spin-up and spin-down are identical, i.e. nonmagnetic), open-shell approach (spin-up and spin-down differs. i.e. magnetized), and various spin-polarized states. The state that shows the minimal total energy considered as the stable magnetic state of that structure. The nanoflakes were optimized on the potential energy surface until the maximum force converges to 1.5×10^{-5} Hartree/Bohr and the RMS density matrix converges to 1.5×10^{-8} Hartree/Bohr. The interaction strength of all the structures (pristine, ternary MPCs, TM-doped ternary MPCs) has been evaluated in terms of their binding energies (E_b), and calculated using the following equations:

$$\mathrm{E_b} = \frac{(\mathrm{n_m\,E_m} + \mathrm{n_x\,E_x} + \mathrm{n_H\,E_H} - \mathrm{E_t})}{\mathrm{n_t}} \tag{1}$$

where n_m, n_x, n_H, and n_t are the number of metals, chalcogens, hydrogens, and total number of atoms, respectively. E_m, E_x, E_H, and E_t are the corresponding energies. The formation energies [11, 12] due to the substitution of 3 chalcogen with P_3 coordination is derived as:

$$E_{\mathrm{sub}} = E_{\mathrm{PQD}} + 3E_{\mathrm{X}} - (E_{\mathrm{pristine}} + 3E_{\mathrm{P}}) \tag{2}$$

where,

- E_{PQD}: Energy of the $M_{12}P_3X_9$ system,
- E_{X}: Isolated energy of chalcogen atoms,
- E_{P}: Isolated energy of phosphorus atoms,
- E_{pristine}: Energy of the $M_{12}X_{12}$ system.

Similarly, the adsorption energy due to the placement of a single transition metal (TM) atom at the hollow site calculated as:

$$E_{\mathrm{int.}} = E_{\mathrm{TMP}} - (E_{\mathrm{PQD}} + E_{\mathrm{TM}}) \tag{3}$$

where,

- E_{TMP}: Total energy of the entire $M_{12}P_3TMX_9$ system,
- E_{TM}: Isolated energy of transition metal atoms.

The calculation of effective g-factor is performed with the Gauge-Including Atomic Orbitals (GIAO) method by applying similar theory. The GIAO technique computes the rotational **g** tensor by taking the second derivative of the ground-state energy (E) with respect to an external magnetic field $\vec{\mathbf{B}}$ propagating in a Cartesian coordinates [13]:

$$\mathrm{g}_{\lambda\eta} = -\frac{\hbar}{\mu_N}\frac{\partial^2 E}{\partial B_\lambda\, \partial J_\eta} \tag{4}$$

where $\hbar$ is the reduced Planck constant, μ_N is the nuclear magneton, J denotes the rotational angular momentum, and λ and η denote the Cartesian lateral (x, y) and vertical (z) directions. The isotropic and anisotropic magnetic susceptibilities are calculated with the Continuous Set of Gauge Transformation (CSGT) method. In practice, it first finds the induced current density $\mathbf{J}(\mathbf{r})$ for the ground state energy (E) with respect to an applied external perturbation **B**. The susceptibility tensor χ_{ij} is then obtained by integrating over all possible gauge origins [14]:

$$\chi_{ij} = \int (\mathbf{r} \times \mathbf{J}(\mathbf{r}))\; d\mathbf{r} \tag{5}$$

The net dipole moment (μ_{avg}), isotropic linear polarizability ($\bar{\alpha}$), and effective first static hyperpolarizability (β_{eff}) were calculated using the Finite Field method with the CAM-B3LYP hybrid exchange-correlation functional [15] due to its ability to compute analytical derivatives, and it has been previously employed in many investigations [16–18]. Although LC-ωPBE functional is a good candidate to compute analytical nuclear gradients $\frac{\partial E}{\partial \mathcal{R}}$, it cannot compute the evaluation of higher-order derivatives with respect to an external perturbation. Thus, to calculate polarizability ($\frac{\partial^2 E}{\partial \mathcal{E}^2}$) or first-hyperpolarizability ($\frac{\partial^3 E}{\partial \mathcal{E}^3}$) using finite-field calculations, one require such functionals capable to perform higher order derivatives and retains essential long-range exchange character. As CAM-B3LYP capable of evaluating $\frac{\partial^n E}{\partial \mathcal{E}^n}$ and has been widely implemented for such finite-field property calculations, it was therefore adopted for the present calculations. An ideal DC limit is considered as an external perturbation for interpreting the optoelectronic responses $\bar{\alpha}(0; 0, 0)$ and $\beta_{\text{eff}}(0; 0, 0)$. In the presence of an electric field, the total energy of the quantum dots can be expanded by means of a Taylor series [19]:

$$\mathrm{E} = \mathrm{E}^0 - \mu_i\, \mathrm{E}_i - \frac{1}{2}\alpha_{ij}\, \mathrm{E}_i\, \mathrm{E}_j - \frac{1}{6}\beta_{ijk}\, \mathrm{E}_i\, \mathrm{E}_j\, \mathrm{E}_k - \ldots \tag{6}$$

Here, E^0 is the ground-state energy of the structures, and μ_i, α_{ij}, and β_{ijk} are the dipole moments, mean polarizability, and first static hyperpolarizability, respectively, with respect to a field perturbation of $\vec{\mathrm{E}}$ along the directions i, j, and $k = x, y, z$ (Cartesian axes). The projected density of states (PDOS) for s, p, and d orbitals, as well as for individual atomic groups, was calculated using molecular orbital energies and coefficients. A Gaussian broadening of $\sigma = 0.3$ eV was applied on a uniform energy grid of 4000 points. Both total and resolved contributions are plotted. States below a 1×10^{-6} a.u. threshold were excluded to avoid numerical noise. Molecular orbital isosurfaces were visualized at ± 0.02 a.u., and the isovalues for spin density and electron density contours were set to 0.0004 a.u.

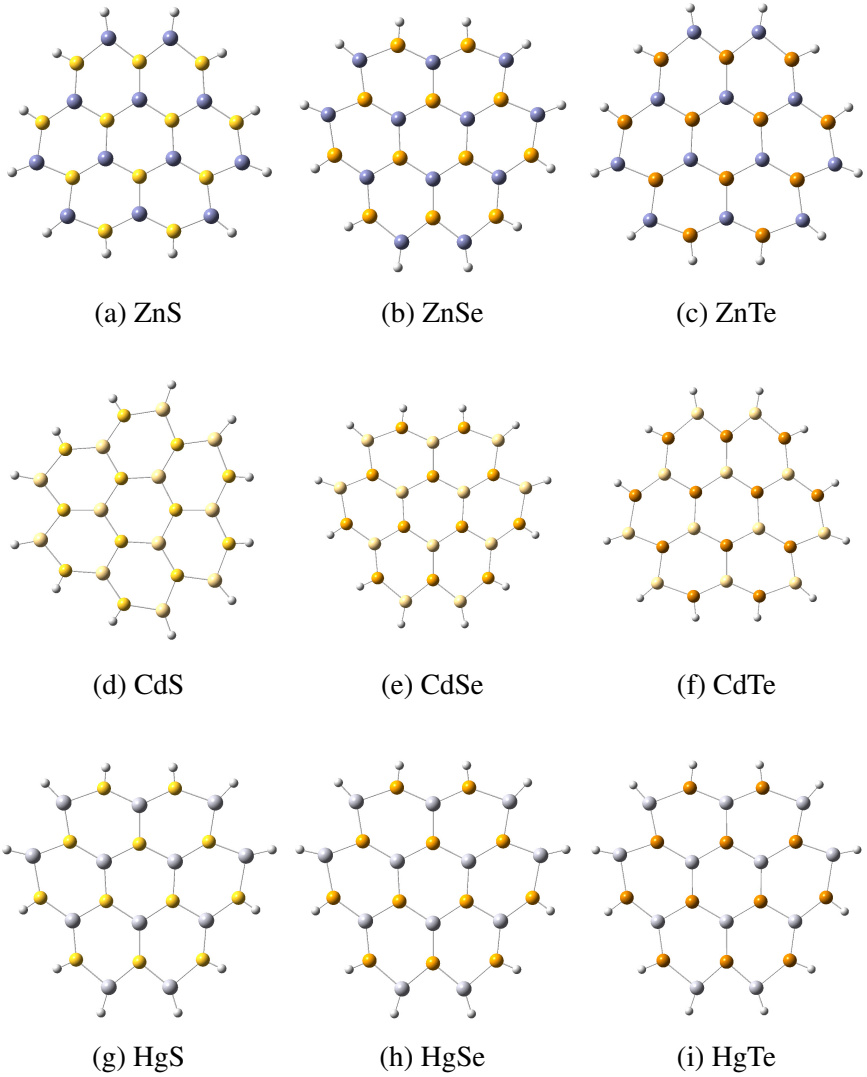

(a) ZnS (b) ZnSe (c) ZnTe

(d) CdS (e) CdSe (f) CdTe

(g) HgS (h) HgSe (i) HgTe

Figure S1: Hexagonal Nanoflakes of Pristine Quantum Dots with Edge Hydrogen Passivation to Prevent Edge Distortion.

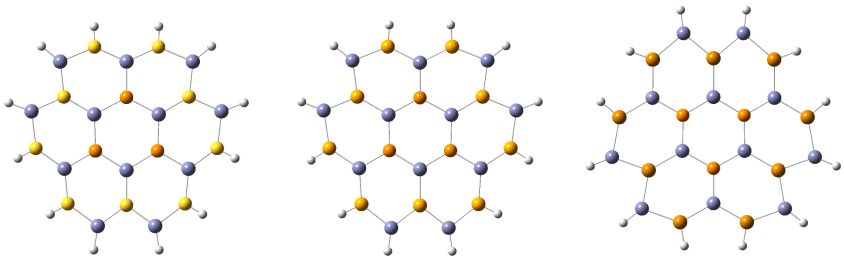

(a) $Zn_{12}P_3S_9$ (b) $Zn_{12}P_3Se_9$ (c) $Zn_{12}P_3Te_9$

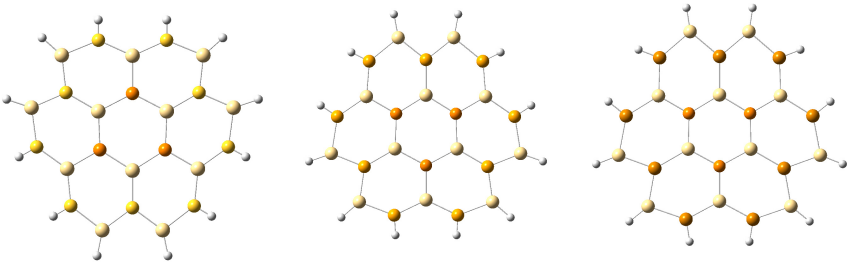

(d) $Cd_{12}P_3S_9$ (e) $Cd_{12}P_3Se_9$ (f) $Cd_{12}P_3Te_9$

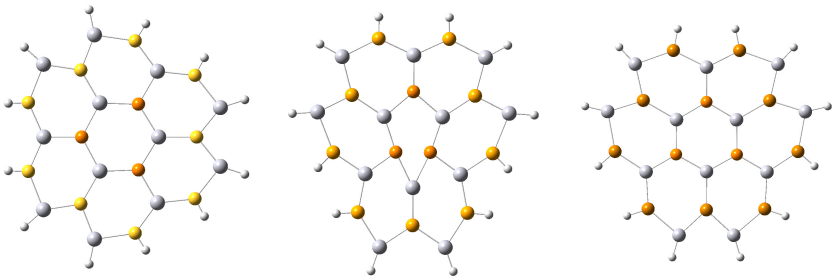

(g) $Hg_{12}P_3S_9$ (h) $Hg_{12}P_3Se_9$ (i) $Hg_{12}P_3Te_9$

Figure S2: Phosphorus-Substituted MPC Quantum Dots Prior to form Localized P–TM Hybridization at Interstitial Sites within the Nanoflakes.

2 Orbital-projected PDOS of Pristine Configurations

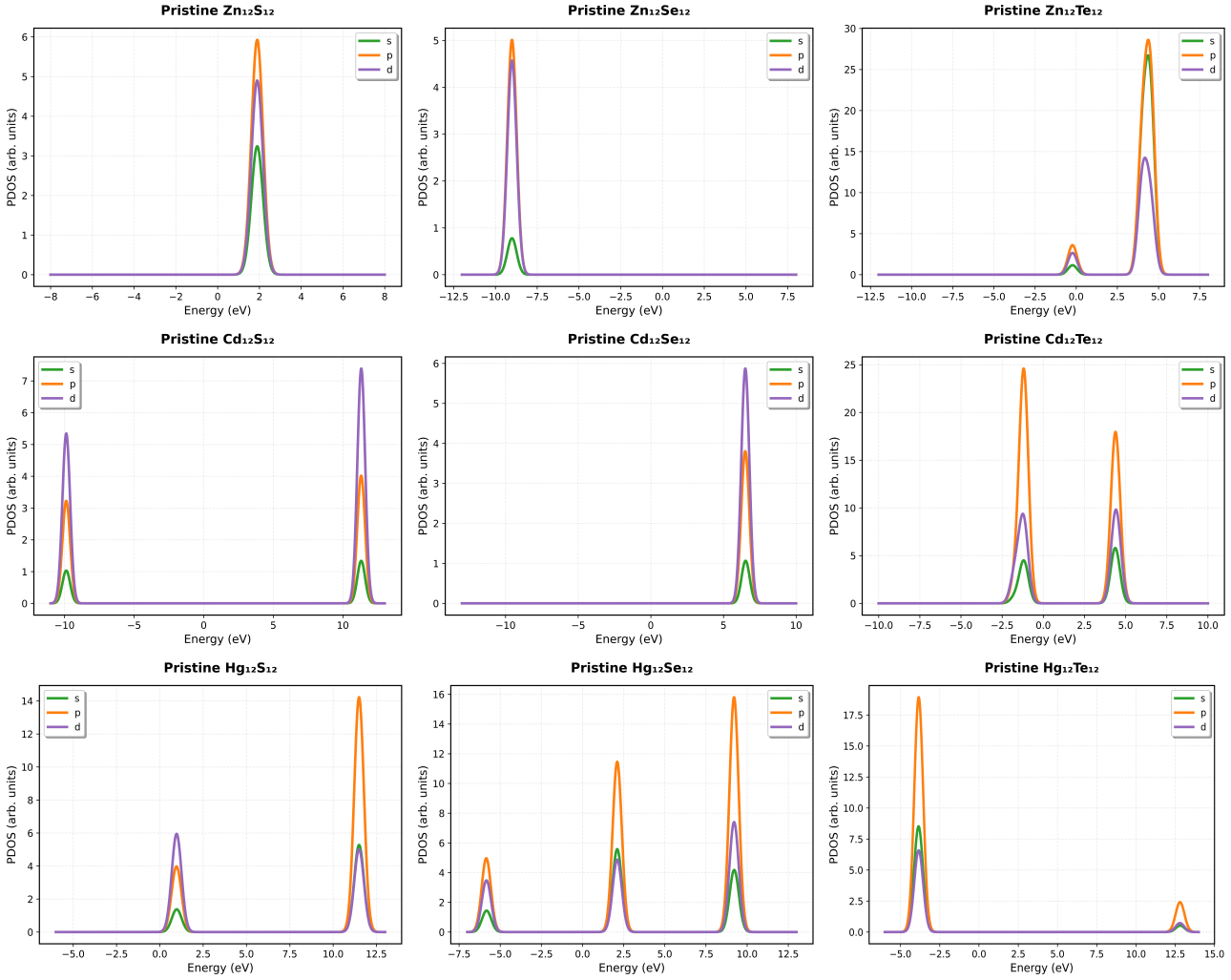

Figure S3: PDOS potted for pristine $M_{12}X_{12}H_{12}$ dots. This shows localized energy states for systems with small metals ($Zn_{12}(S/Se)_{12}$), that results in a wide energy gap (E_g = 7.37/6.56 eV). The systems with larger metal-chalcogen combination depicts a denser energy spectrum due to their larger atomic radii, which makes the electronic distributions more diffuse and result in a lower energy gap (2.70–4.77 eV).

3 Element-projected PDOS of Interstitial Confinement

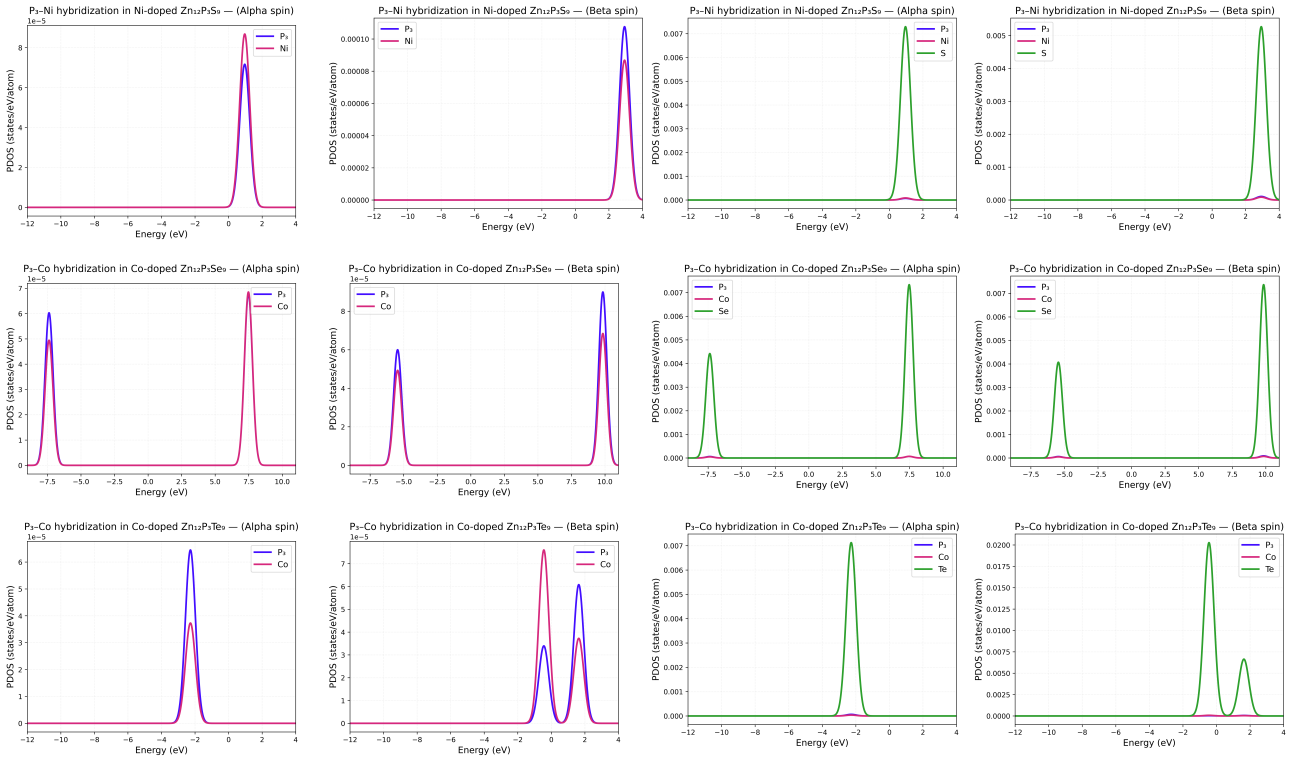

(a)

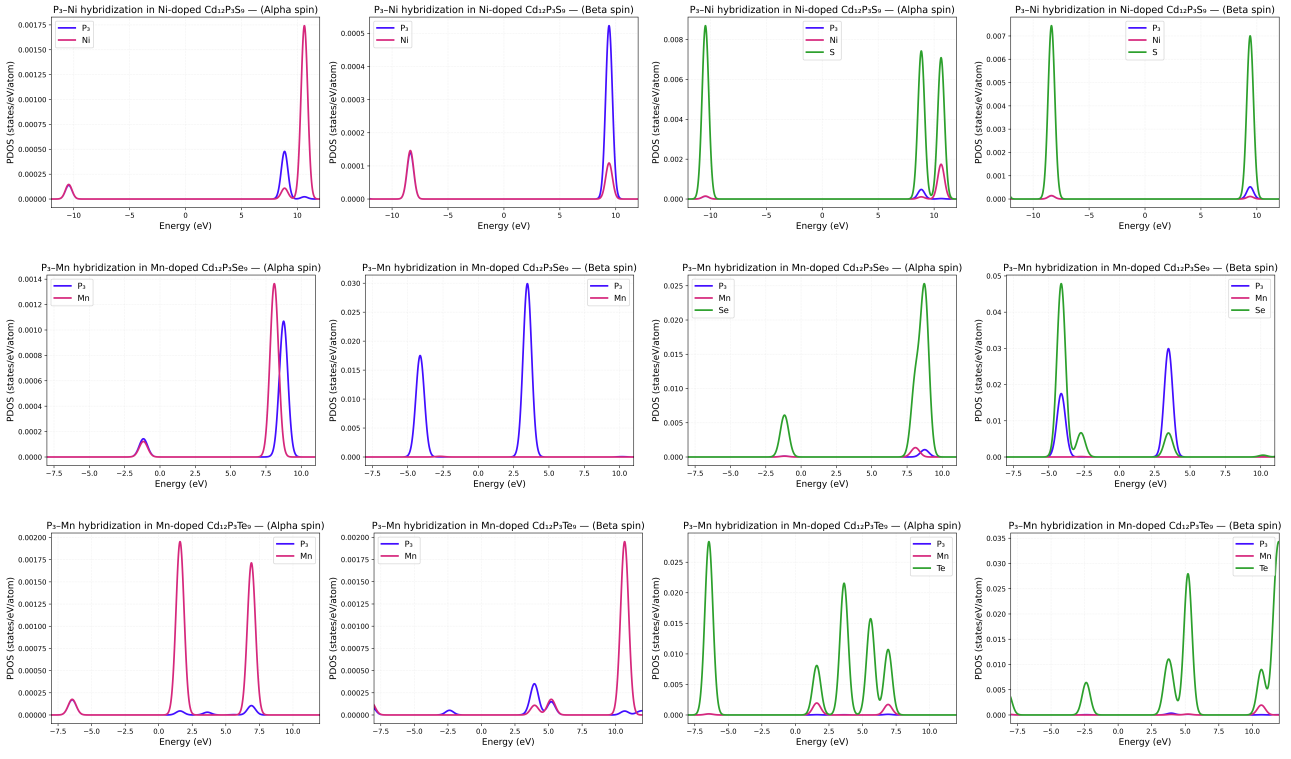

(b)

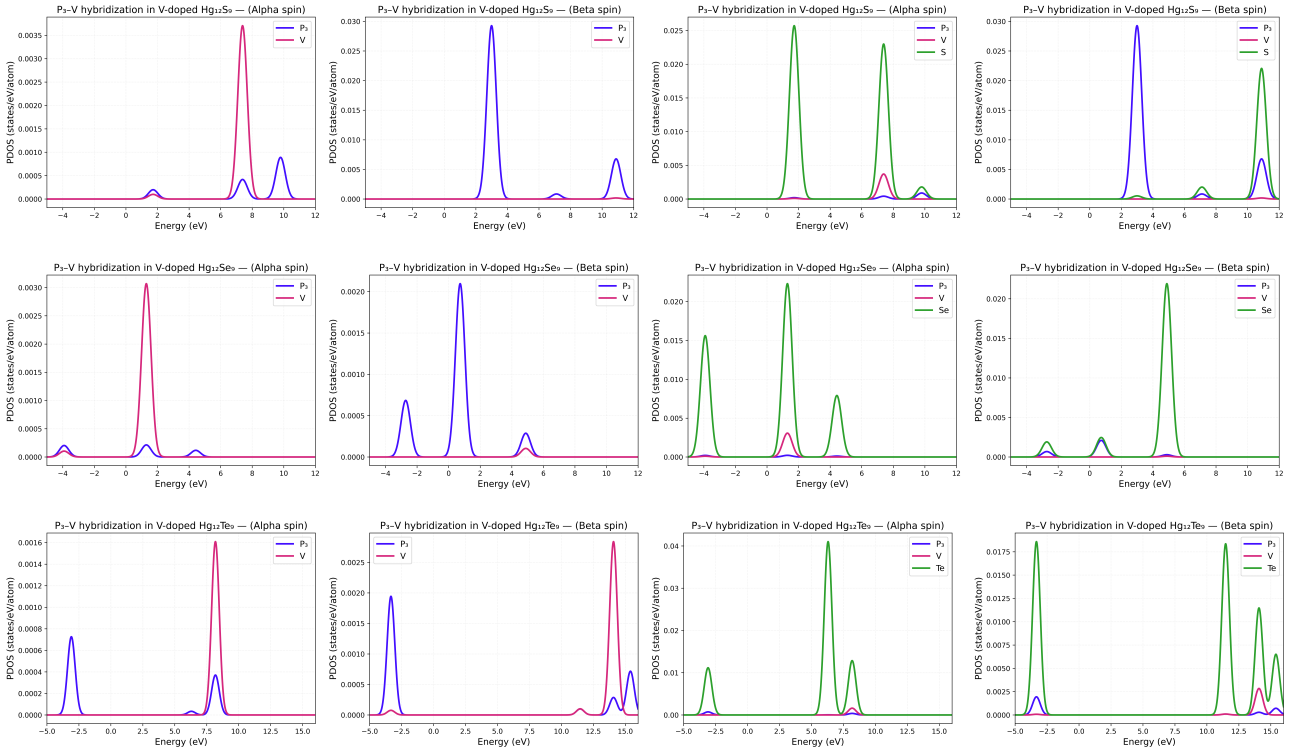

(c)

Figure S4(a–c): Atom-specific PDOS plotted side-by-side to show P_3–TM pairing and how this pairing interacts with the P_3–TM–X_9 indirect bonding of chalcogens for both spin channels. As discussed, the chalcogens modulate the hybridization strength of each interstitial pair in a host configuration, which causes them to adopt either the lowest, or consistently highest magnetic configuration. The β-channel and α-channel electronic states of P_3–Ni/Mn/V hybridize asymmetrically with the S/Se/Te, that offers selective tuning of one spin-channel, control over the effective magnetic moment, and the response magnitude of the first static hyperpolarizability.

4 Vibrational Response Analysis

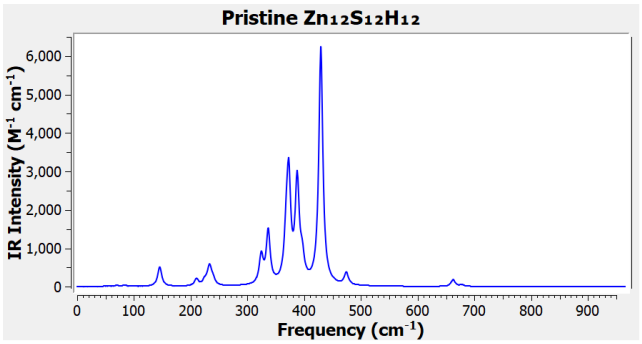

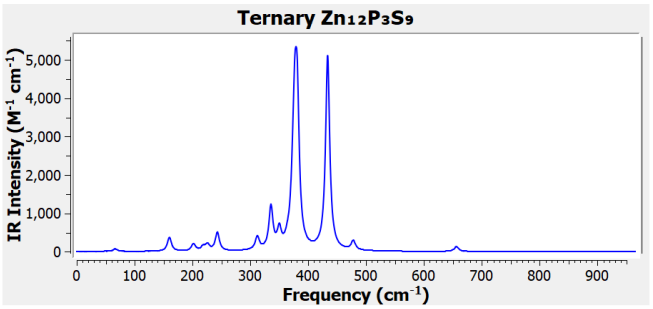

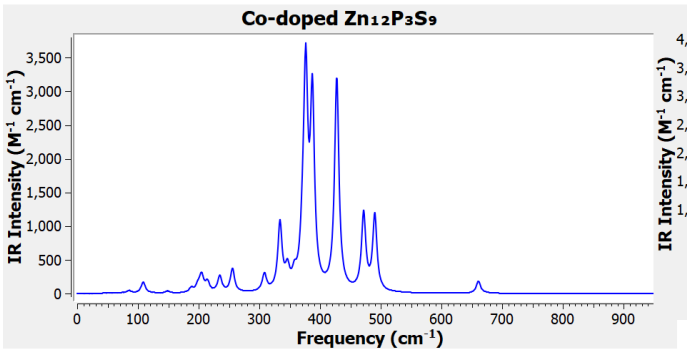

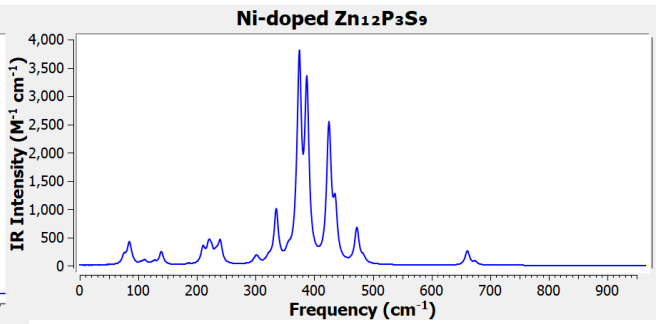

5a

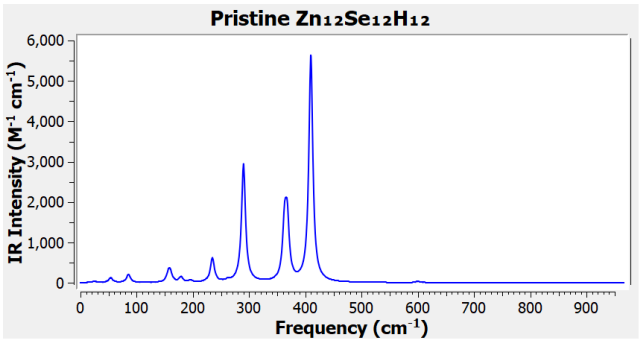

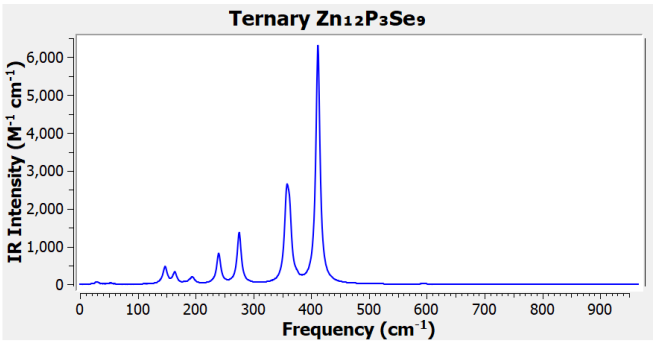

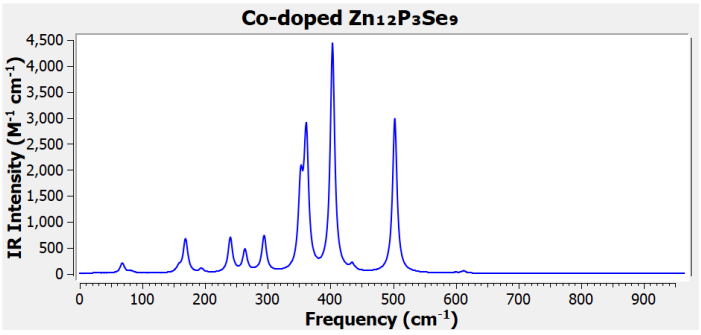

5b

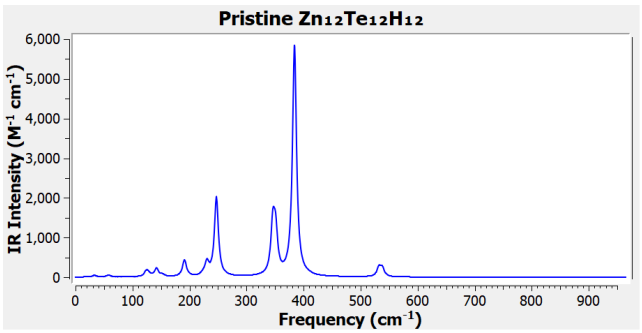
Pristine Zn12Te12H12
IR Intensity (M-1 cm-1)
Frequency (cm-1)

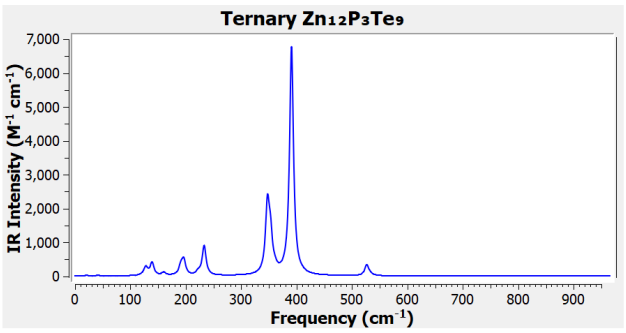
Ternary Zn12P3Te9
IR Intensity (M-1 cm-1)
Frequency (cm-1)

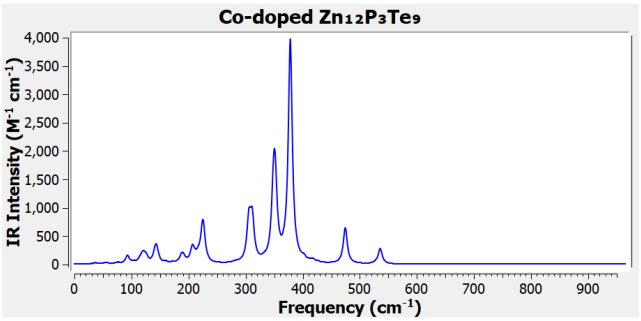
Co-doped Zn12P3Te9
IR Intensity (M-1 cm-1)
Frequency (cm-1)

5c

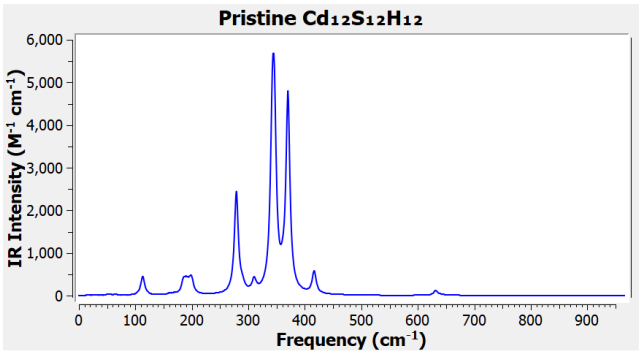
Pristine Cd12S12H12
IR Intensity (M-1 cm-1)
Frequency (cm-1)

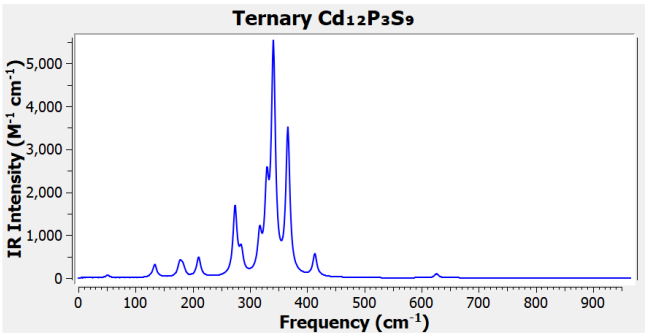
Ternary Cd12P3S9
IR Intensity (M-1 cm-1)
Frequency (cm-1)

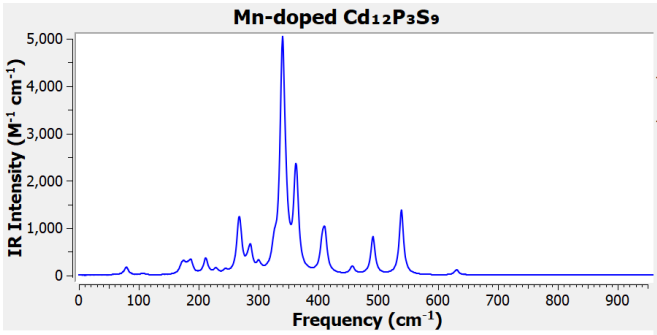
Mn-doped Cd12P3S9
IR Intensity (M-1 cm-1)
Frequency (cm-1)

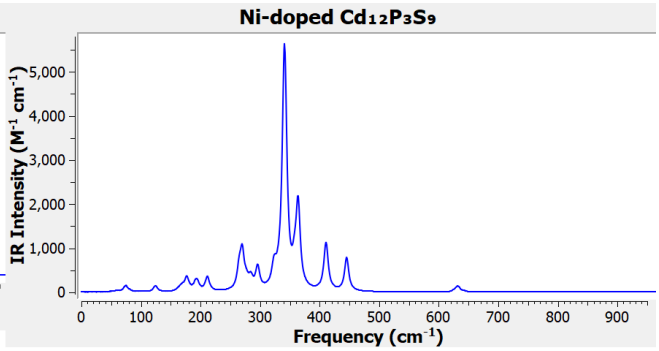
Ni-doped Cd12P3S9
IR Intensity (M-1 cm-1)
Frequency (cm-1)

5d

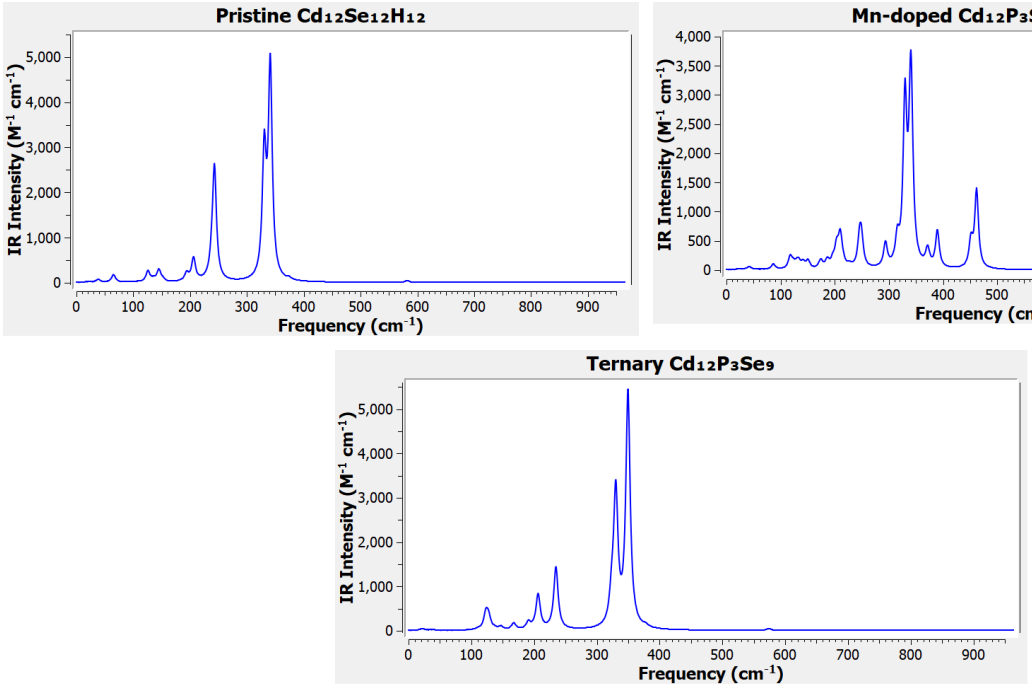
Pristine Cd12Se12H12
IR Intensity (M-1 cm-1)
Frequency (cm-1)
Mn-doped Cd12P3Se9
IR Intensity (M-1 cm-1)
Frequency (cm-1)
Ternary Cd12P3Se9
IR Intensity (M-1 cm-1)
Frequency (cm-1)

5e

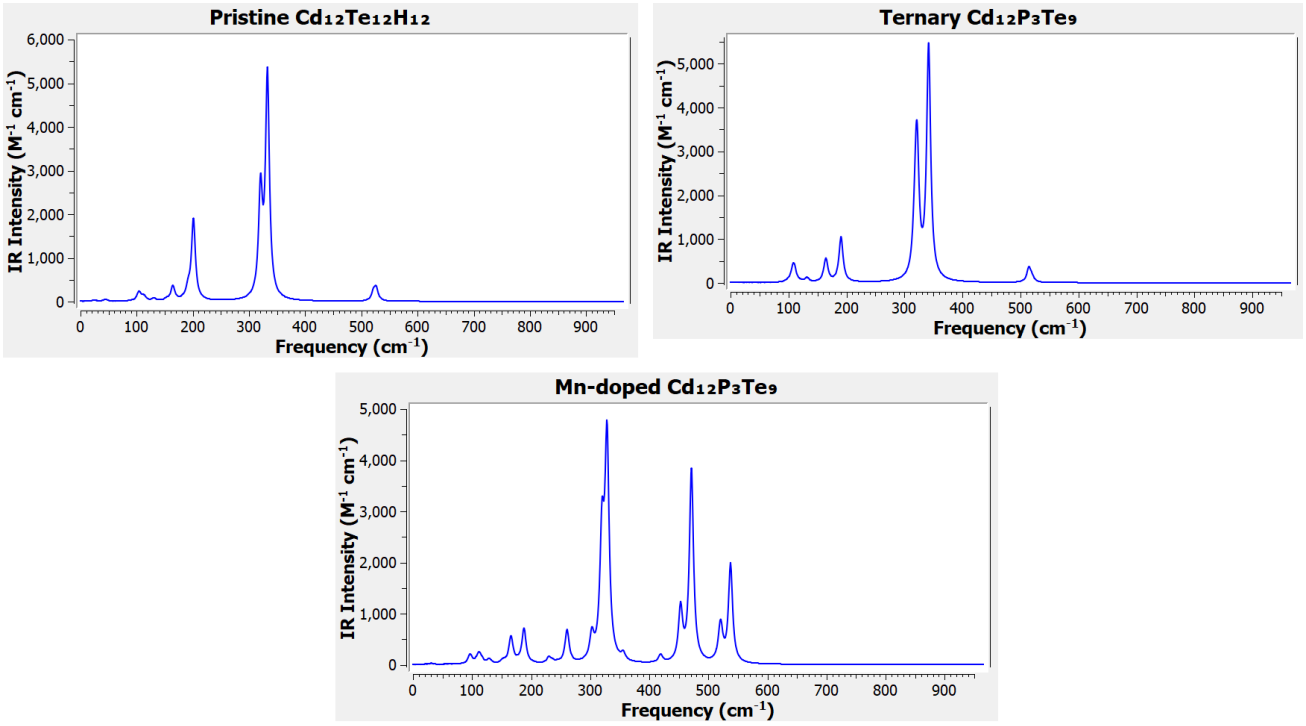
Pristine Cd12Te12H12
IR Intensity (M-1 cm-1)
Frequency (cm-1)
Ternary Cd12P3Te9
IR Intensity (M-1 cm-1)
Frequency (cm-1)
Mn-doped Cd12P3Te9
IR Intensity (M-1 cm-1)
Frequency (cm-1)

5f

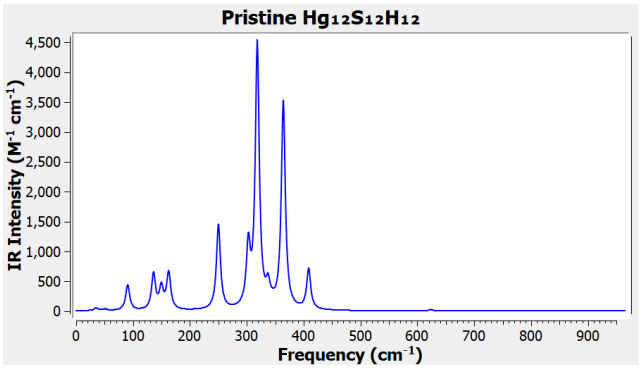
Pristine Hg12S12H12
IR Intensity (M-1 cm-1)
Frequency (cm-1)

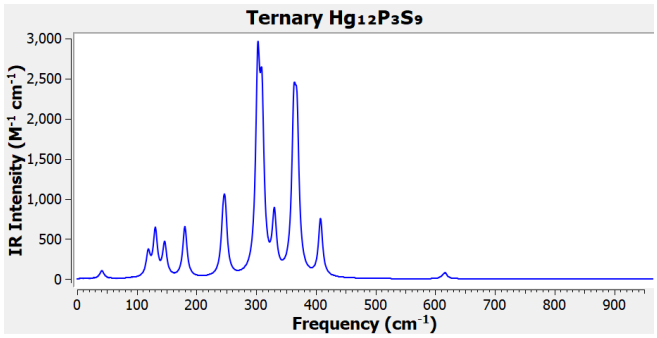
Ternary Hg12P3S9
IR Intensity (M-1 cm-1)
Frequency (cm-1)

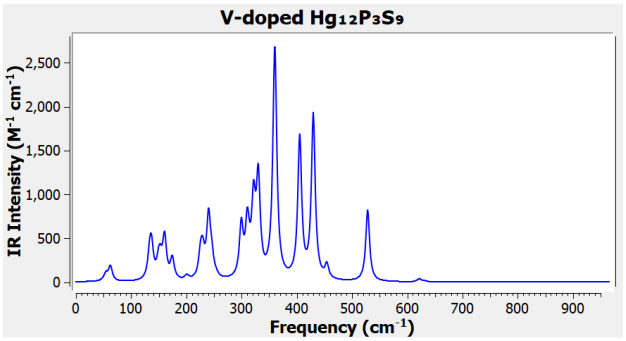
V-doped Hg12P3S9
IR Intensity (M-1 cm-1)
Frequency (cm-1)

5g

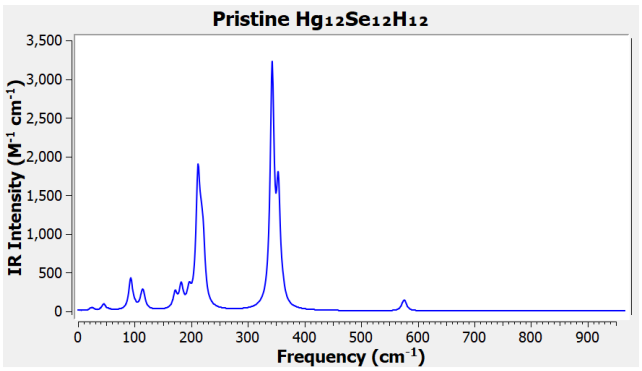
Pristine Hg12Se12H12
IR Intensity (M-1 cm-1)
Frequency (cm-1)

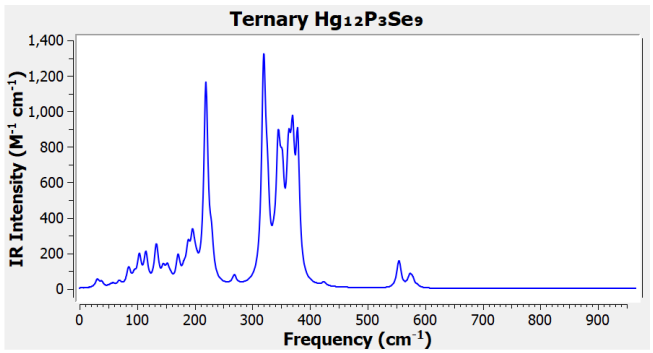
Ternary Hg12P3Se9
IR Intensity (M-1 cm-1)
Frequency (cm-1)

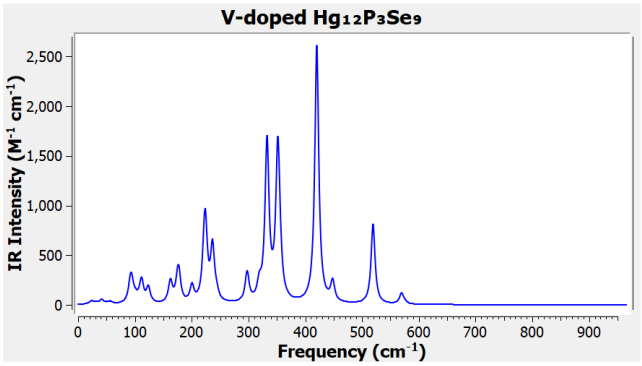
V-doped Hg12P3Se9
IR Intensity (M-1 cm-1)
Frequency (cm-1)

5h

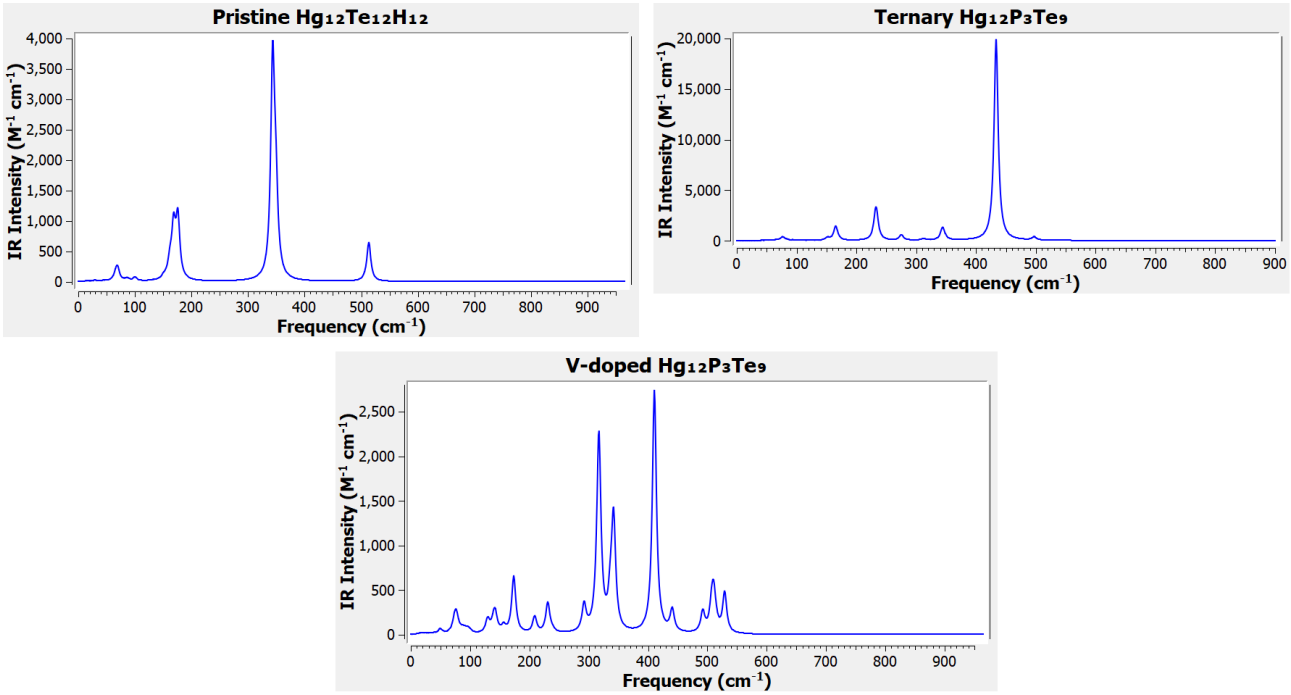

5i

Figure S5 (a–i): The IR spectra of the pristine, ternary, and interstitially doped nanodots are presented for each of the group. This analysis shows that all the vibrational frequencies are real, with no imaginary vibrations, which ensures the systems occupy stable minima on the potential energy landscape and indicates structural stability.

5 Energetic and Bonding Response under Finite-Temperature Perturbations

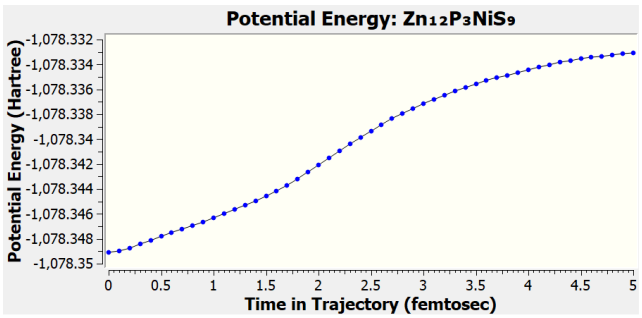

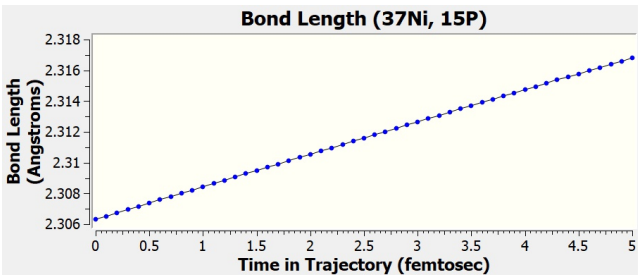

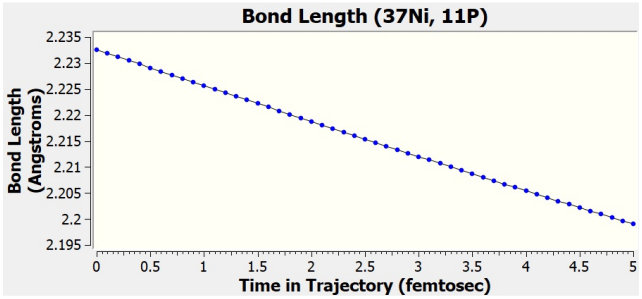

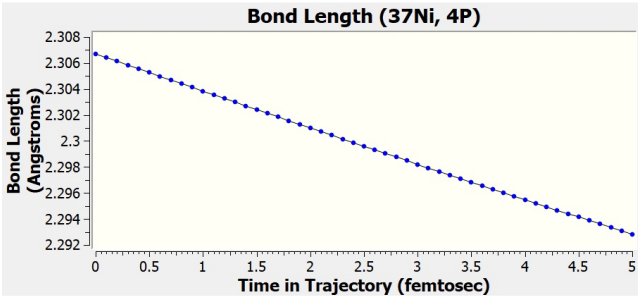

6a

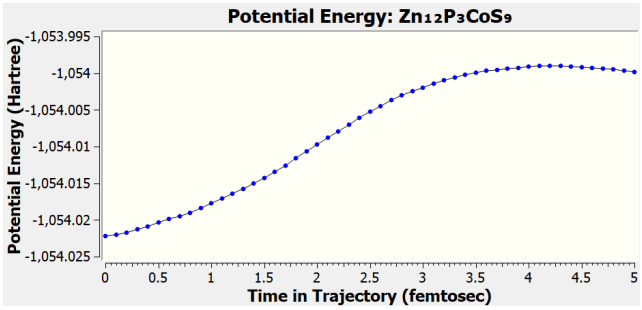

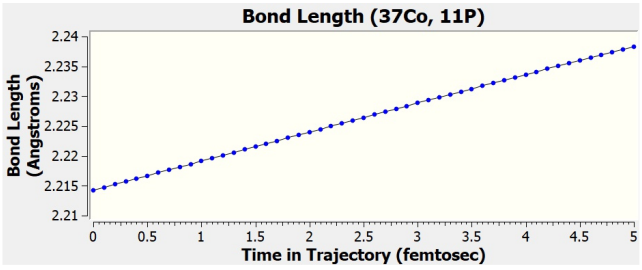

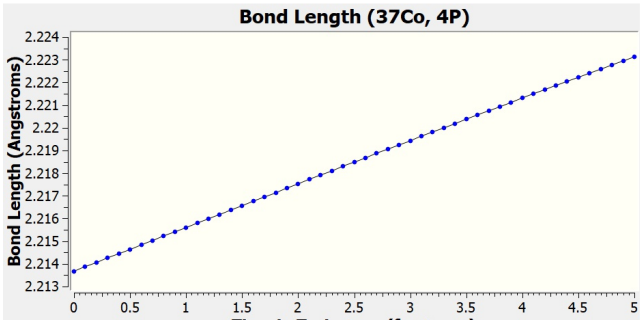

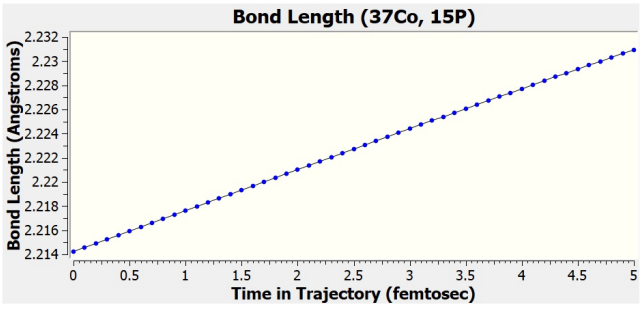

6b

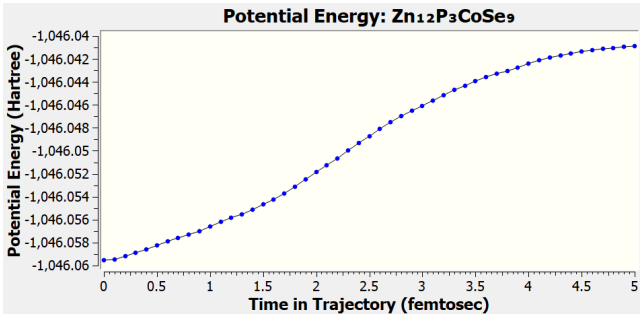
Potential Energy: Zn12P3CoSe9
Potential Energy (Hartree)
-1,046.04
-1,046.042
-1,046.044
-1,046.046
-1,046.048
-1,046.05
-1,046.052
-1,046.054
-1,046.056
-1,046.058
-1,046.06
0 0.5 1 1.5 2 2.5 3 3.5 4 4.5 5
Time in Trajectory (femtosec)

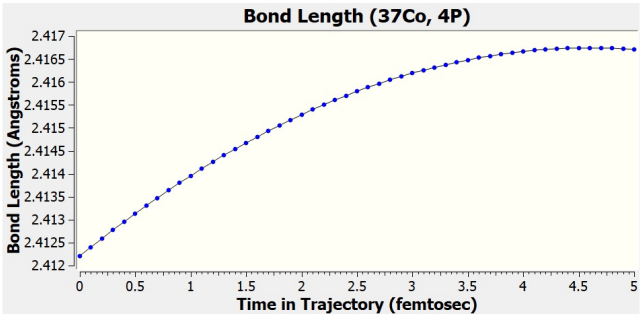
Bond Length (37Co, 4P)
Bond Length (Angstroms)
2.417
2.4165
2.416
2.4155
2.415
2.4145
2.414
2.4135
2.413
2.4125
2.412
0 0.5 1 1.5 2 2.5 3 3.5 4 4.5 5
Time in Trajectory (femtosec)

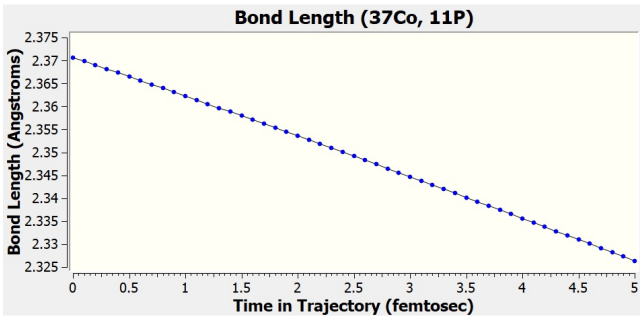
Bond Length (37Co, 11P)
Bond Length (Angstroms)
2.375
2.37
2.365
2.36
2.355
2.35
2.345
2.34
2.335
2.33
2.325
0 0.5 1 1.5 2 2.5 3 3.5 4 4.5 5
Time in Trajectory (femtosec)

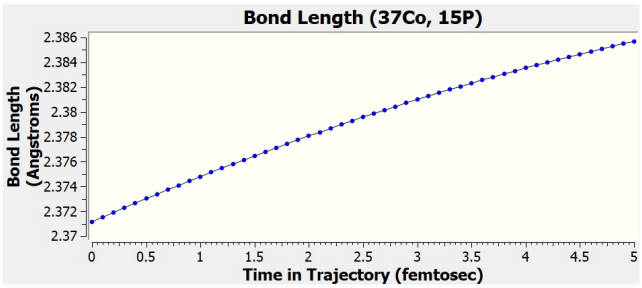
Bond Length (37Co, 15P)
Bond Length (Angstroms)
2.386
2.384
2.382
2.38
2.378
2.376
2.374
2.372
2.37
0 0.5 1 1.5 2 2.5 3 3.5 4 4.5 5
Time in Trajectory (femtosec)

6c

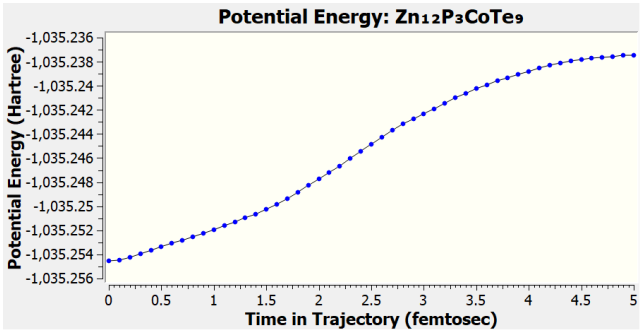
Potential Energy: Zn12P3CoTe9
Potential Energy (Hartree)
-1,035.236
-1,035.238
-1,035.24
-1,035.242
-1,035.244
-1,035.246
-1,035.248
-1,035.25
-1,035.252
-1,035.254
-1,035.256
0 0.5 1 1.5 2 2.5 3 3.5 4 4.5 5
Time in Trajectory (femtosec)

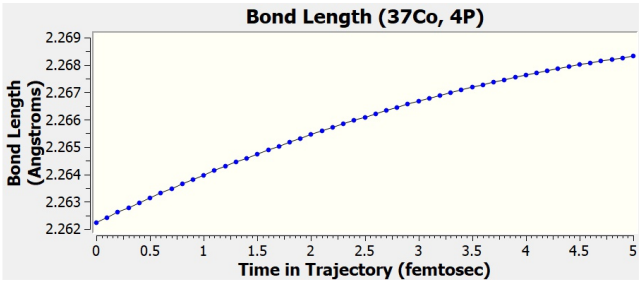
Bond Length (37Co, 4P)
Bond Length (Angstroms)
2.269
2.268
2.267
2.266
2.265
2.264
2.263
2.262
0 0.5 1 1.5 2 2.5 3 3.5 4 4.5 5
Time in Trajectory (femtosec)

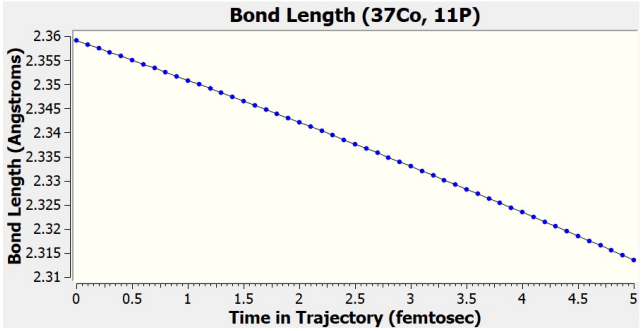
Bond Length (37Co, 11P)
Bond Length (Angstroms)
2.36
2.355
2.35
2.345
2.34
2.335
2.33
2.325
2.32
2.315
2.31
0 0.5 1 1.5 2 2.5 3 3.5 4 4.5 5
Time in Trajectory (femtosec)

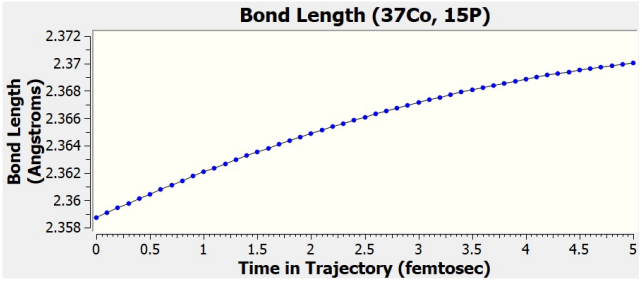
Bond Length (37Co, 15P)
Bond Length (Angstroms)
2.372
2.37
2.368
2.366
2.364
2.362
2.36
2.358
0 0.5 1 1.5 2 2.5 3 3.5 4 4.5 5
Time in Trajectory (femtosec)

6d

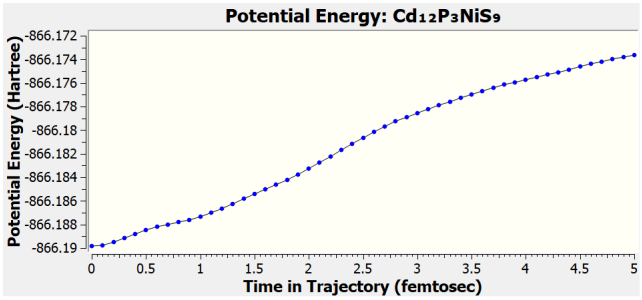
Potential Energy: Cd12P3NiS9
Potential Energy (Hartree)
-866.172
-866.174
-866.176
-866.178
-866.18
-866.182
-866.184
-866.186
-866.188
-866.19
0 0.5 1 1.5 2 2.5 3 3.5 4 4.5 5
Time in Trajectory (femtosec)

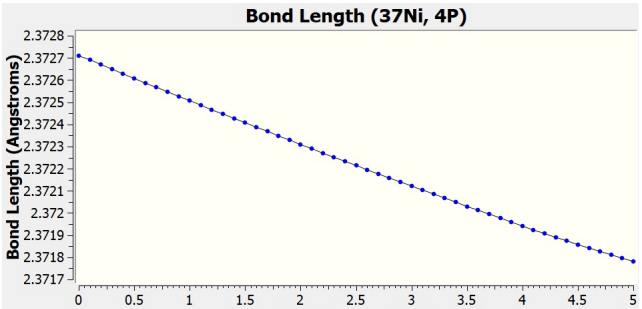
Bond Length (37Ni, 4P)
Bond Length (Angstroms)
2.3728
2.3727
2.3726
2.3725
2.3724
2.3723
2.3722
2.3721
2.372
2.3719
2.3718
2.3717
0 0.5 1 1.5 2 2.5 3 3.5 4 4.5 5

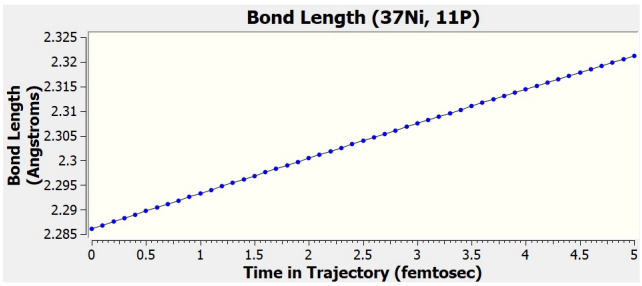
Bond Length (37Ni, 11P)
Bond Length (Angstroms)
2.325
2.32
2.315
2.31
2.305
2.3
2.295
2.29
2.285
0 0.5 1 1.5 2 2.5 3 3.5 4 4.5 5
Time in Trajectory (femtosec)

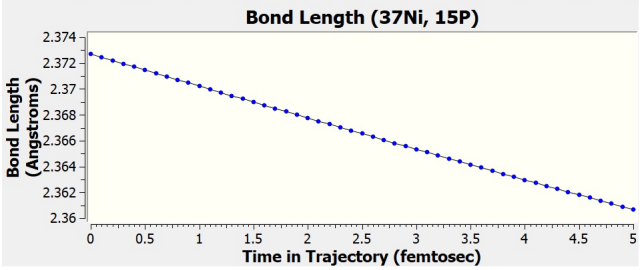
Bond Length (37Ni, 15P)
Bond Length (Angstroms)
2.374
2.372
2.37
2.368
2.366
2.364
2.362
2.36
0 0.5 1 1.5 2 2.5 3 3.5 4 4.5 5
Time in Trajectory (femtosec)

6e

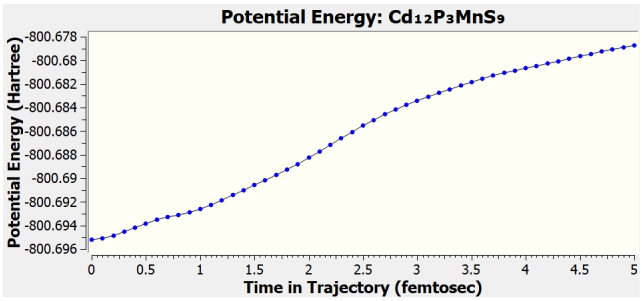
Potential Energy: Cd12P3MnS9
Potential Energy (Hartree)
-800.678
-800.68
-800.682
-800.684
-800.686
-800.688
-800.69
-800.692
-800.694
-800.696
0 0.5 1 1.5 2 2.5 3 3.5 4 4.5 5
Time in Trajectory (femtosec)

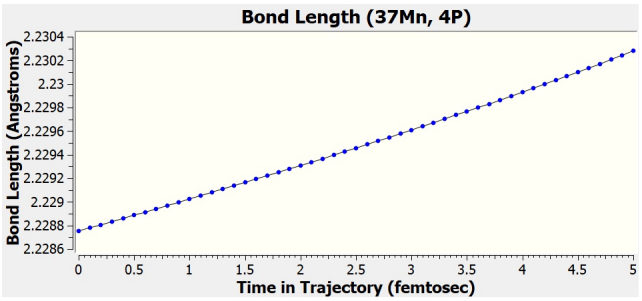
Bond Length (37Mn, 4P)
Bond Length (Angstroms)
2.2304
2.2302
2.23
2.2298
2.2296
2.2294
2.2292
2.229
2.2288
2.2286
0 0.5 1 1.5 2 2.5 3 3.5 4 4.5 5
Time in Trajectory (femtosec)

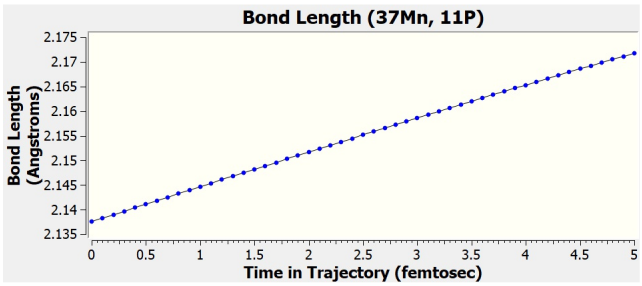
Bond Length (37Mn, 11P)
Bond Length (Angstroms)
2.175
2.17
2.165
2.16
2.155
2.15
2.145
2.14
2.135
0 0.5 1 1.5 2 2.5 3 3.5 4 4.5 5
Time in Trajectory (femtosec)

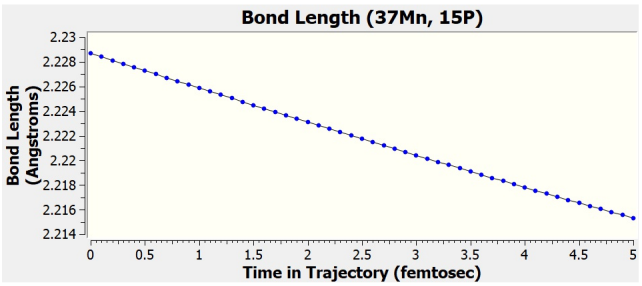
Bond Length (37Mn, 15P)
Bond Length (Angstroms)
2.23
2.228
2.226
2.224
2.222
2.22
2.218
2.216
2.214
0 0.5 1 1.5 2 2.5 3 3.5 4 4.5 5
Time in Trajectory (femtosec)

6f

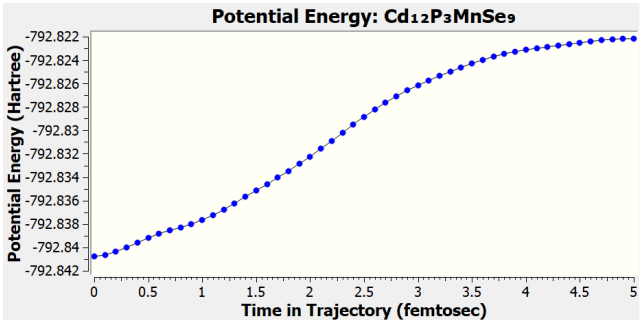
Potential Energy: Cd12P3MnSe9
Potential Energy (Hartree)
-792.822
-792.824
-792.826
-792.828
-792.83
-792.832
-792.834
-792.836
-792.838
-792.84
-792.842
0 0.5 1 1.5 2 2.5 3 3.5 4 4.5 5
Time in Trajectory (femtosec)

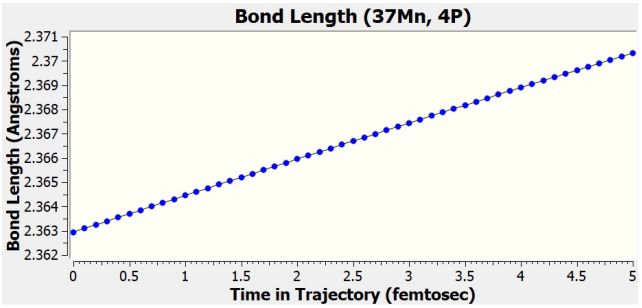
Bond Length (37Mn, 4P)
Bond Length (Angstroms)
2.371
2.37
2.369
2.368
2.367
2.366
2.365
2.364
2.363
2.362
0 0.5 1 1.5 2 2.5 3 3.5 4 4.5 5
Time in Trajectory (femtosec)

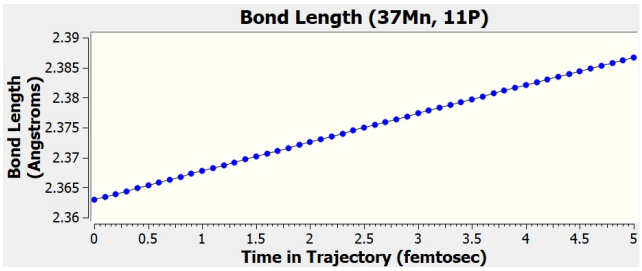
Bond Length (37Mn, 11P)
Bond Length (Angstroms)
2.39
2.385
2.38
2.375
2.37
2.365
2.36
0 0.5 1 1.5 2 2.5 3 3.5 4 4.5 5
Time in Trajectory (femtosec)

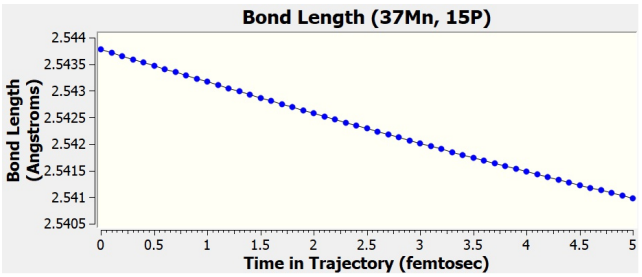
Bond Length (37Mn, 15P)
Bond Length (Angstroms)
2.544
2.5435
2.543
2.5425
2.542
2.5415
2.541
2.5405
0 0.5 1 1.5 2 2.5 3 3.5 4 4.5 5
Time in Trajectory (femtosec)

6g

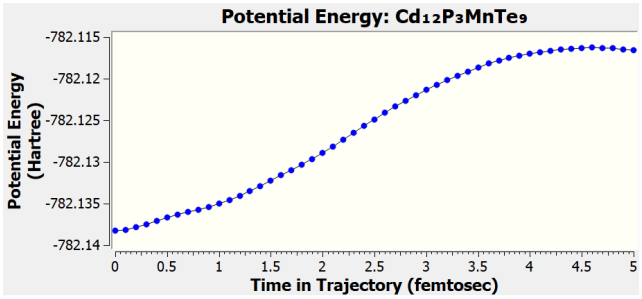
Potential Energy: Cd12P3MnTe9
Potential Energy (Hartree)
-782.115
-782.12
-782.125
-782.13
-782.135
-782.14
0 0.5 1 1.5 2 2.5 3 3.5 4 4.5 5
Time in Trajectory (femtosec)

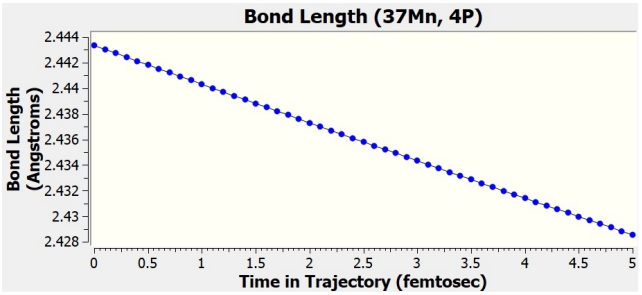
Bond Length (37Mn, 4P)
Bond Length (Angstroms)
2.444
2.442
2.44
2.438
2.436
2.434
2.432
2.43
2.428
0 0.5 1 1.5 2 2.5 3 3.5 4 4.5 5
Time in Trajectory (femtosec)

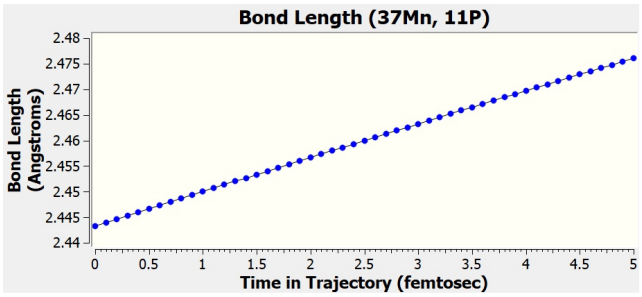
Bond Length (37Mn, 11P)
Bond Length (Angstroms)
2.48
2.475
2.47
2.465
2.46
2.455
2.45
2.445
2.44
0 0.5 1 1.5 2 2.5 3 3.5 4 4.5 5
Time in Trajectory (femtosec)

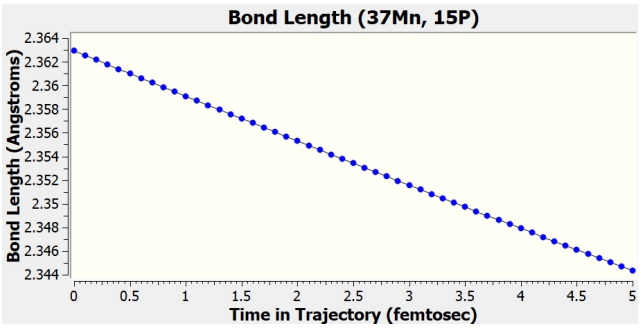
Bond Length (37Mn, 15P)
Bond Length (Angstroms)
2.364
2.362
2.36
2.358
2.356
2.354
2.352
2.35
2.348
2.346
2.344
0 0.5 1 1.5 2 2.5 3 3.5 4 4.5 5
Time in Trajectory (femtosec)

6h

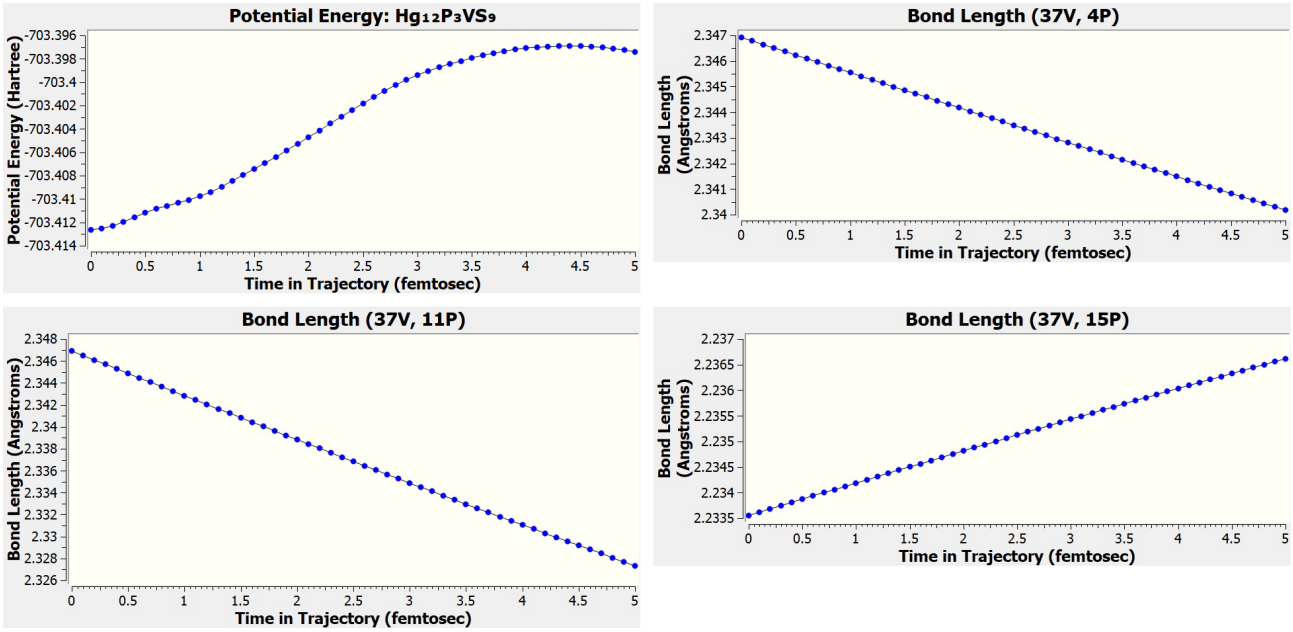
Potential Energy: Hg12P3VS9
Potential Energy (Hartree)
Time in Trajectory (femtosec)
Bond Length (37V, 4P)
Bond Length (Angstroms)
Time in Trajectory (femtosec)
Bond Length (37V, 11P)
Bond Length (Angstroms)
Time in Trajectory (femtosec)
Bond Length (37V, 15P)
Bond Length (Angstroms)
Time in Trajectory (femtosec)

6i

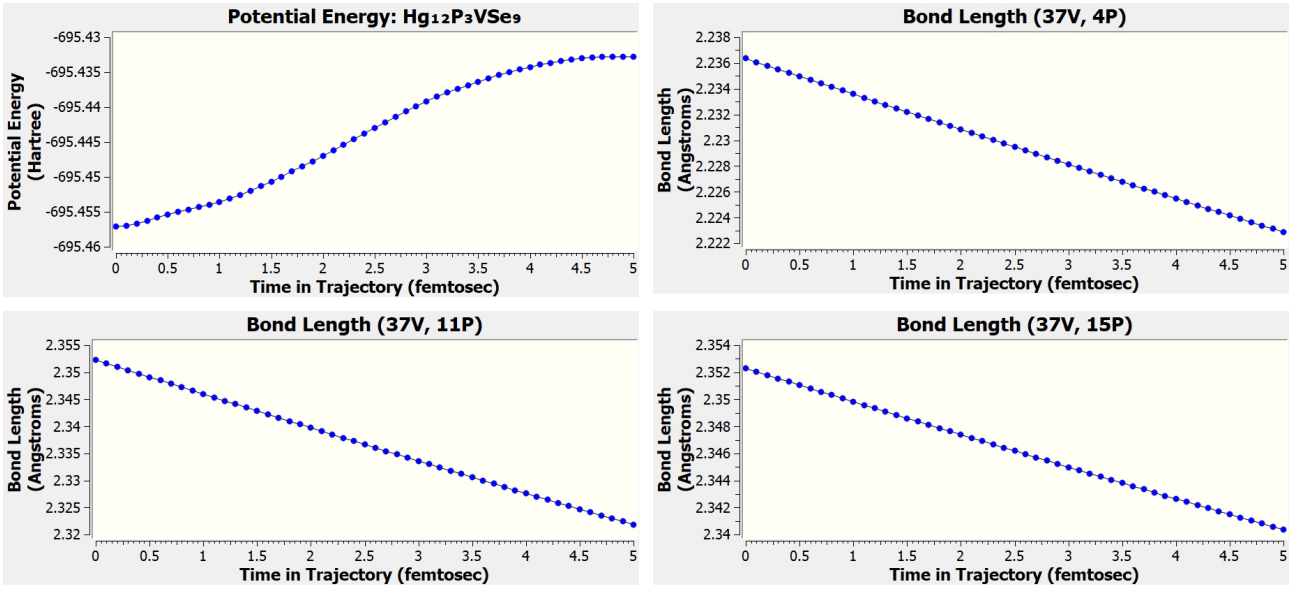
Potential Energy: Hg12P3VSe9
Potential Energy (Hartree)
Time in Trajectory (femtosec)
Bond Length (37V, 4P)
Bond Length (Angstroms)
Time in Trajectory (femtosec)
Bond Length (37V, 11P)
Bond Length (Angstroms)
Time in Trajectory (femtosec)
Bond Length (37V, 15P)
Bond Length (Angstroms)
Time in Trajectory (femtosec)

6j

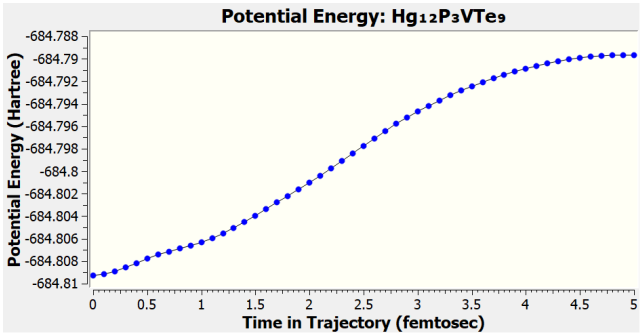
Potential Energy: Hg12P3VTe9
Potential Energy (Hartree)
-684.788
-684.79
-684.792
-684.794
-684.796
-684.798
-684.8
-684.802
-684.804
-684.806
-684.808
-684.81
0 0.5 1 1.5 2 2.5 3 3.5 4 4.5 5
Time in Trajectory (femtosec)

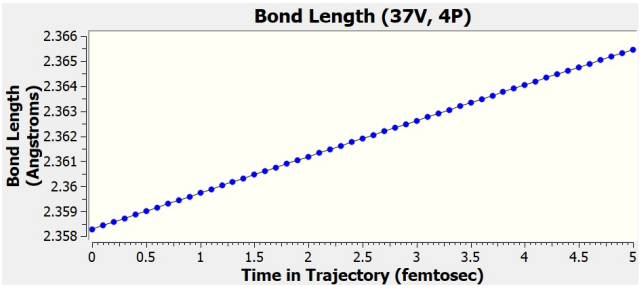
Bond Length (37V, 4P)
Bond Length (Angstroms)
2.366
2.365
2.364
2.363
2.362
2.361
2.36
2.359
2.358
0 0.5 1 1.5 2 2.5 3 3.5 4 4.5 5
Time in Trajectory (femtosec)

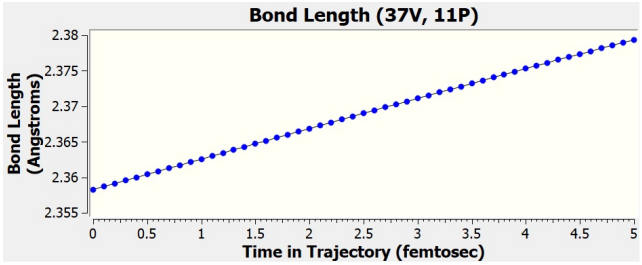
Bond Length (37V, 11P)
Bond Length (Angstroms)
2.38
2.375
2.37
2.365
2.36
2.355
0 0.5 1 1.5 2 2.5 3 3.5 4 4.5 5
Time in Trajectory (femtosec)

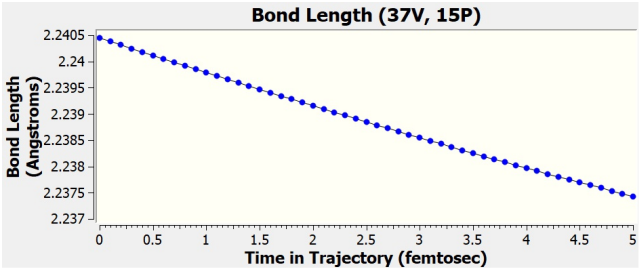
Bond Length (37V, 15P)
Bond Length (Angstroms)
2.2405
2.24
2.2395
2.239
2.2385
2.238
2.2375
2.237
0 0.5 1 1.5 2 2.5 3 3.5 4 4.5 5
Time in Trajectory (femtosec)

6k

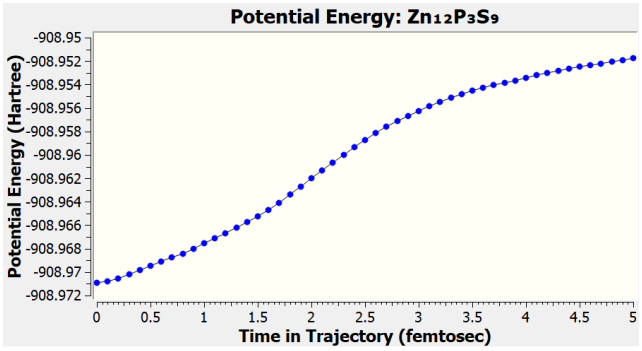
Potential Energy: Zn12P3S9
Potential Energy (Hartree)
-908.95
-908.952
-908.954
-908.956
-908.958
-908.96
-908.962
-908.964
-908.966
-908.968
-908.97
-908.972
0 0.5 1 1.5 2 2.5 3 3.5 4 4.5 5
Time in Trajectory (femtosec)

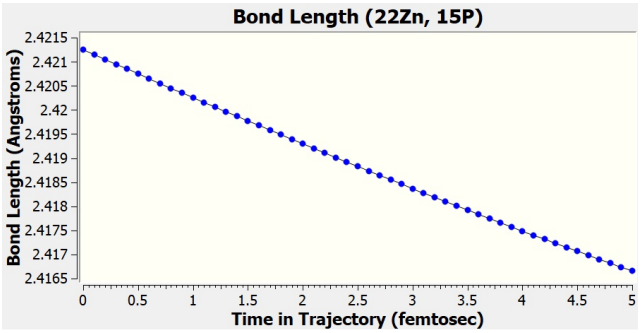
Bond Length (22Zn, 15P)
Bond Length (Angstroms)
2.4215
2.421
2.4205
2.42
2.4195
2.419
2.4185
2.418
2.4175
2.417
2.4165
0 0.5 1 1.5 2 2.5 3 3.5 4 4.5 5
Time in Trajectory (femtosec)

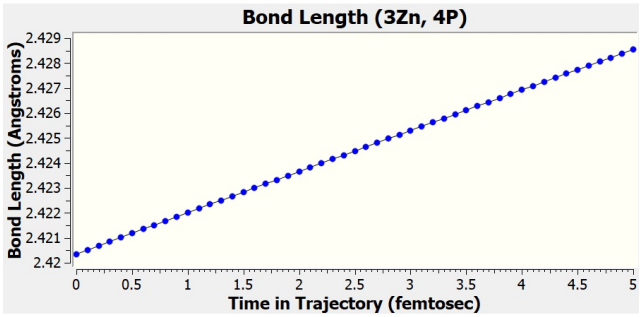
Bond Length (3Zn, 4P)
Bond Length (Angstroms)
2.429
2.428
2.427
2.426
2.425
2.424
2.423
2.422
2.421
2.42
0 0.5 1 1.5 2 2.5 3 3.5 4 4.5 5
Time in Trajectory (femtosec)

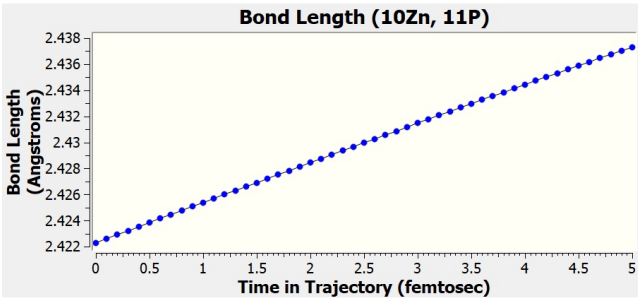
Bond Length (10Zn, 11P)
Bond Length (Angstroms)
2.438
2.436
2.434
2.432
2.43
2.428
2.426
2.424
2.422
0 0.5 1 1.5 2 2.5 3 3.5 4 4.5 5
Time in Trajectory (femtosec)

6l

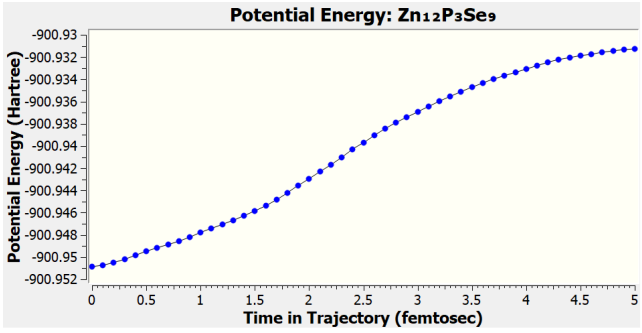
Potential Energy: Zn12P3Se9
Potential Energy (Hartree)
-900.93
-900.932
-900.934
-900.936
-900.938
-900.94
-900.942
-900.944
-900.946
-900.948
-900.95
-900.952
0 0.5 1 1.5 2 2.5 3 3.5 4 4.5 5
Time in Trajectory (femtosec)

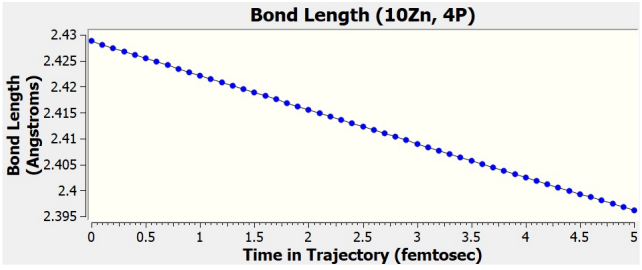
Bond Length (10Zn, 4P)
Bond Length (Angstroms)
2.43
2.425
2.42
2.415
2.41
2.405
2.4
2.395
0 0.5 1 1.5 2 2.5 3 3.5 4 4.5 5
Time in Trajectory (femtosec)

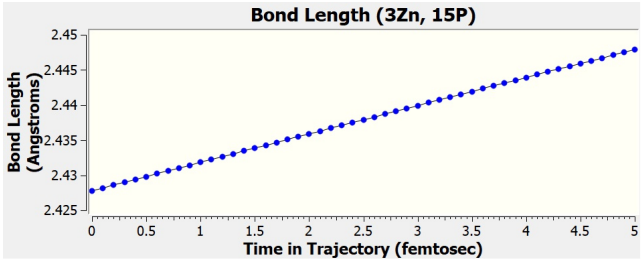
Bond Length (3Zn, 15P)
Bond Length (Angstroms)
2.45
2.445
2.44
2.435
2.43
2.425
0 0.5 1 1.5 2 2.5 3 3.5 4 4.5 5
Time in Trajectory (femtosec)

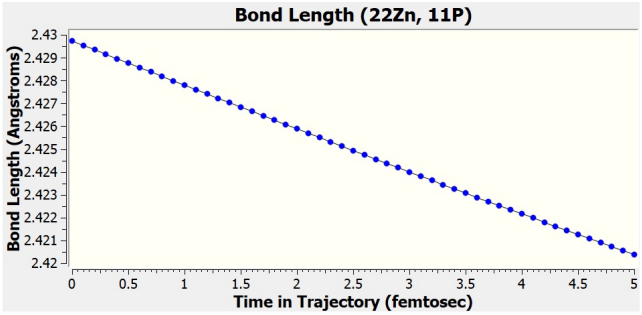
Bond Length (22Zn, 11P)
Bond Length (Angstroms)
2.43
2.429
2.428
2.427
2.426
2.425
2.424
2.423
2.422
2.421
2.42
0 0.5 1 1.5 2 2.5 3 3.5 4 4.5 5
Time in Trajectory (femtosec)

6m

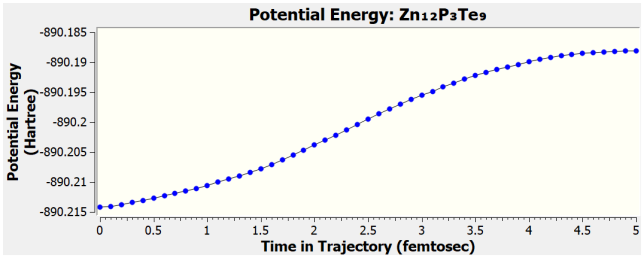
Potential Energy: Zn12P3Te9
Potential Energy (Hartree)
-890.185
-890.19
-890.195
-890.2
-890.205
-890.21
-890.215
0 0.5 1 1.5 2 2.5 3 3.5 4 4.5 5
Time in Trajectory (femtosec)

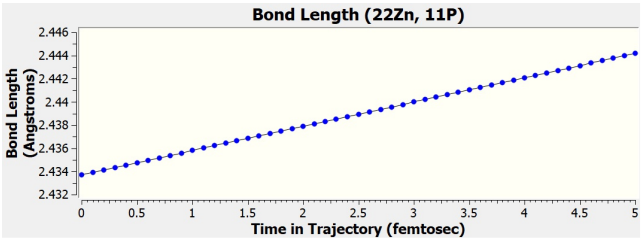
Bond Length (22Zn, 11P)
Bond Length (Angstroms)
2.446
2.444
2.442
2.44
2.438
2.436
2.434
2.432
0 0.5 1 1.5 2 2.5 3 3.5 4 4.5 5
Time in Trajectory (femtosec)

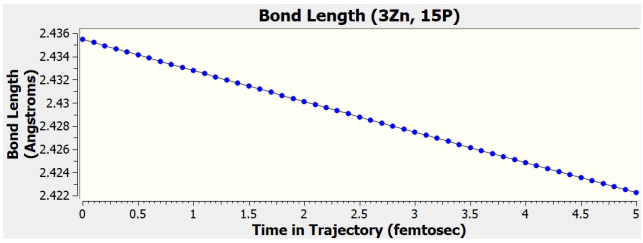
Bond Length (3Zn, 15P)
Bond Length (Angstroms)
2.436
2.434
2.432
2.43
2.428
2.426
2.424
2.422
0 0.5 1 1.5 2 2.5 3 3.5 4 4.5 5
Time in Trajectory (femtosec)

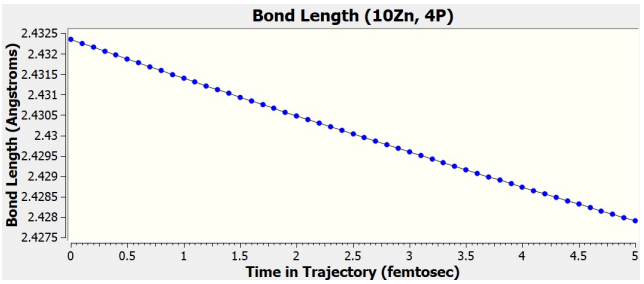
Bond Length (10Zn, 4P)
Bond Length (Angstroms)
2.4325
2.432
2.4315
2.431
2.4305
2.43
2.4295
2.429
2.4285
2.428
2.4275
0 0.5 1 1.5 2 2.5 3 3.5 4 4.5 5
Time in Trajectory (femtosec)

6n

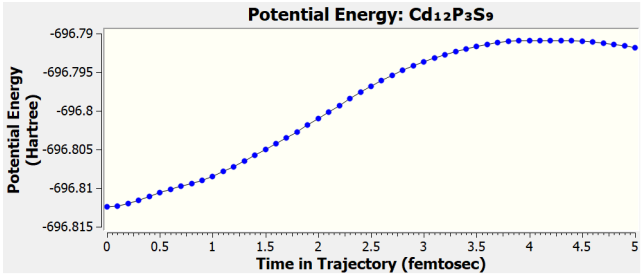
Potential Energy: Cd12P3S9
Potential Energy (Hartree)
-696.79
-696.795
-696.8
-696.805
-696.81
-696.815
0 0.5 1 1.5 2 2.5 3 3.5 4 4.5 5
Time in Trajectory (femtosec)

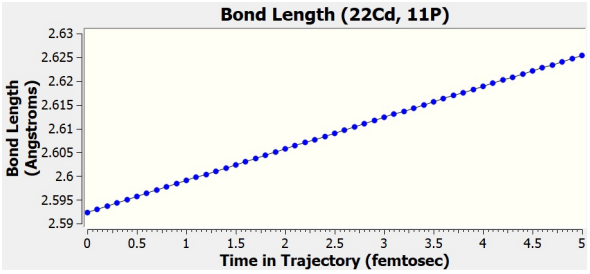
Bond Length (22Cd, 11P)
Bond Length (Angstroms)
2.63
2.625
2.62
2.615
2.61
2.605
2.6
2.595
2.59
0 0.5 1 1.5 2 2.5 3 3.5 4 4.5 5
Time in Trajectory (femtosec)

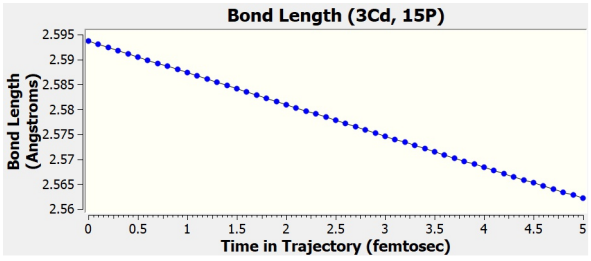
Bond Length (3Cd, 15P)
Bond Length (Angstroms)
2.595
2.59
2.585
2.58
2.575
2.57
2.565
2.56
0 0.5 1 1.5 2 2.5 3 3.5 4 4.5 5
Time in Trajectory (femtosec)

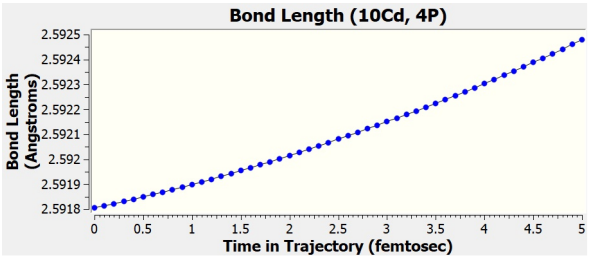
Bond Length (10Cd, 4P)
Bond Length (Angstroms)
2.5925
2.5924
2.5923
2.5922
2.5921
2.592
2.5919
2.5918
0 0.5 1 1.5 2 2.5 3 3.5 4 4.5 5
Time in Trajectory (femtosec)

6o

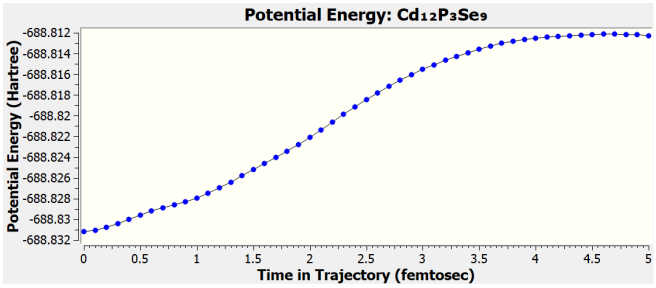
Potential Energy: Cd12P3Se9
Potential Energy (Hartree)
-688.812
-688.814
-688.816
-688.818
-688.82
-688.822
-688.824
-688.826
-688.828
-688.83
-688.832
0 0.5 1 1.5 2 2.5 3 3.5 4 4.5 5
Time in Trajectory (femtosec)

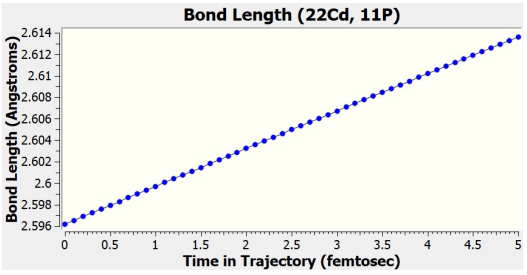
Bond Length (22Cd, 11P)
Bond Length (Angstroms)
2.614
2.612
2.61
2.608
2.606
2.604
2.602
2.6
2.598
2.596
0 0.5 1 1.5 2 2.5 3 3.5 4 4.5 5
Time in Trajectory (femtosec)

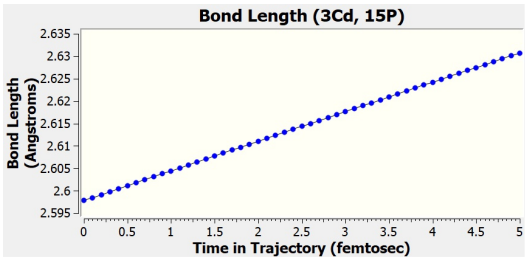
Bond Length (3Cd, 15P)
Bond Length (Angstroms)
2.635
2.63
2.625
2.62
2.615
2.61
2.605
2.6
2.595
0 0.5 1 1.5 2 2.5 3 3.5 4 4.5 5
Time in Trajectory (femtosec)

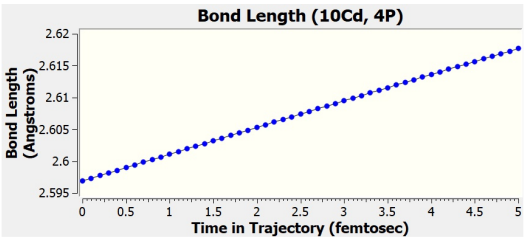
Bond Length (10Cd, 4P)
Bond Length (Angstroms)
2.62
2.615
2.61
2.605
2.6
2.595
0 0.5 1 1.5 2 2.5 3 3.5 4 4.5 5
Time in Trajectory (femtosec)

6p

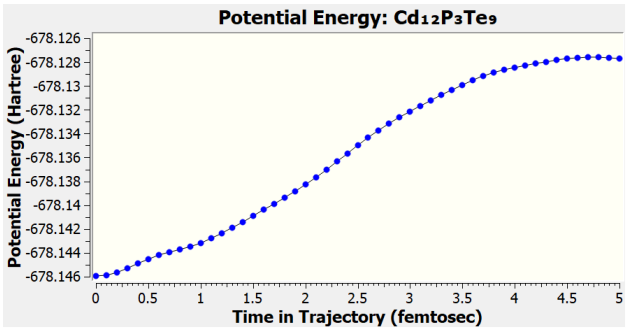
Potential Energy: Cd12P3Te9
Potential Energy (Hartree)
-678.126
-678.128
-678.13
-678.132
-678.134
-678.136
-678.138
-678.14
-678.142
-678.144
-678.146
0 0.5 1 1.5 2 2.5 3 3.5 4 4.5 5
Time in Trajectory (femtosec)

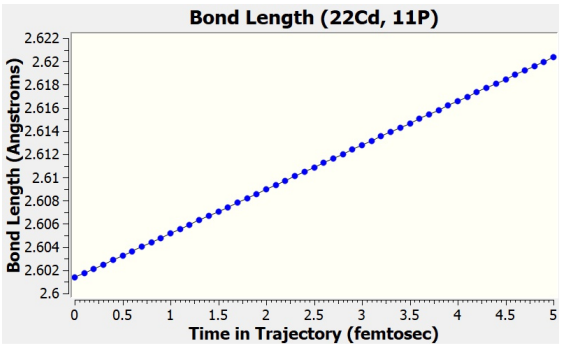
Bond Length (22Cd, 11P)
Bond Length (Angstroms)
2.622
2.62
2.618
2.616
2.614
2.612
2.61
2.608
2.606
2.604
2.602
2.6
0 0.5 1 1.5 2 2.5 3 3.5 4 4.5 5
Time in Trajectory (femtosec)

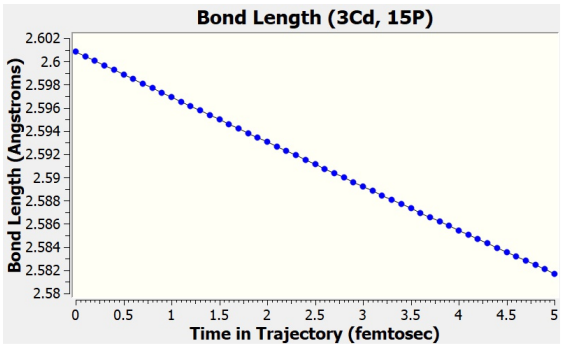
Bond Length (3Cd, 15P)
Bond Length (Angstroms)
2.602
2.6
2.598
2.596
2.594
2.592
2.59
2.588
2.586
2.584
2.582
2.58
0 0.5 1 1.5 2 2.5 3 3.5 4 4.5 5
Time in Trajectory (femtosec)

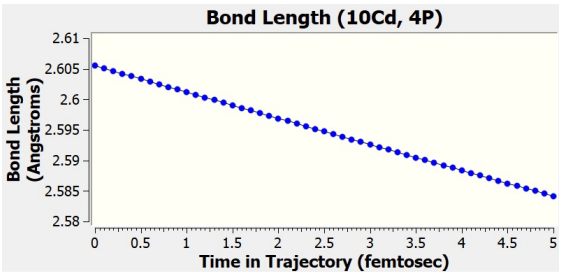
Bond Length (10Cd, 4P)
Bond Length (Angstroms)
2.61
2.605
2.6
2.595
2.59
2.585
2.58
0 0.5 1 1.5 2 2.5 3 3.5 4 4.5 5
Time in Trajectory (femtosec)

6q

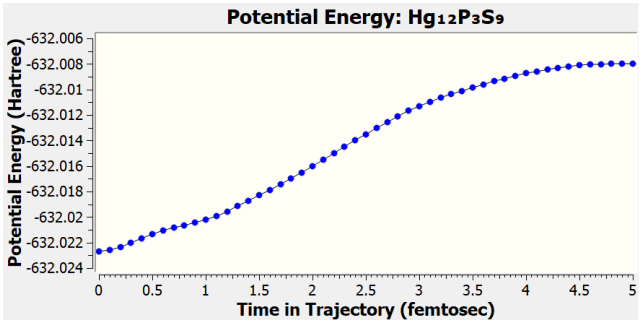
Potential Energy: Hg12P3S9
Potential Energy (Hartree)
-632.006
-632.008
-632.01
-632.012
-632.014
-632.016
-632.018
-632.02
-632.022
-632.024
0 0.5 1 1.5 2 2.5 3 3.5 4 4.5 5
Time in Trajectory (femtosec)

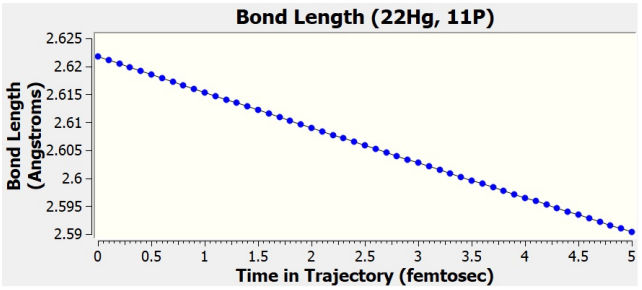
Bond Length (22Hg, 11P)
Bond Length (Angstroms)
2.625
2.62
2.615
2.61
2.605
2.6
2.595
2.59
0 0.5 1 1.5 2 2.5 3 3.5 4 4.5 5
Time in Trajectory (femtosec)

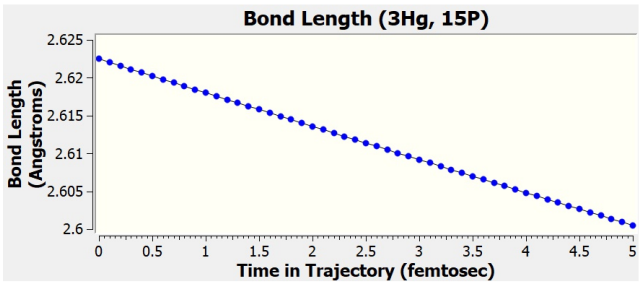
Bond Length (3Hg, 15P)
Bond Length (Angstroms)
2.625
2.62
2.615
2.61
2.605
2.6
0 0.5 1 1.5 2 2.5 3 3.5 4 4.5 5
Time in Trajectory (femtosec)

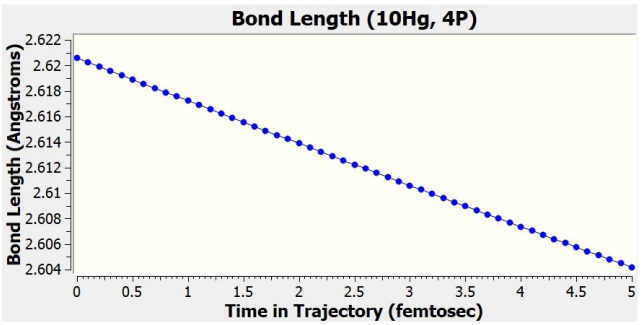
Bond Length (10Hg, 4P)
Bond Length (Angstroms)
2.622
2.62
2.618
2.616
2.614
2.612
2.61
2.608
2.606
2.604
0 0.5 1 1.5 2 2.5 3 3.5 4 4.5 5
Time in Trajectory (femtosec)

6r

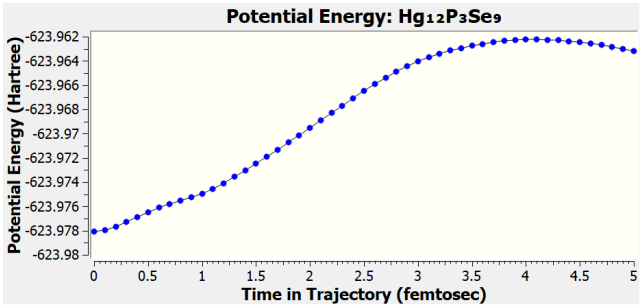
Potential Energy: Hg12P3Se9
Potential Energy (Hartree)
-623.962
-623.964
-623.966
-623.968
-623.97
-623.972
-623.974
-623.976
-623.978
-623.98
0 0.5 1 1.5 2 2.5 3 3.5 4 4.5 5
Time in Trajectory (femtosec)

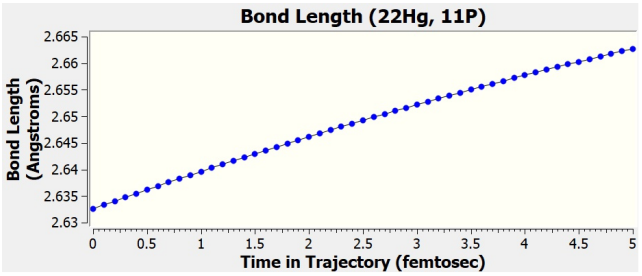
Bond Length (22Hg, 11P)
Bond Length (Angstroms)
2.665
2.66
2.655
2.65
2.645
2.64
2.635
2.63
0 0.5 1 1.5 2 2.5 3 3.5 4 4.5 5
Time in Trajectory (femtosec)

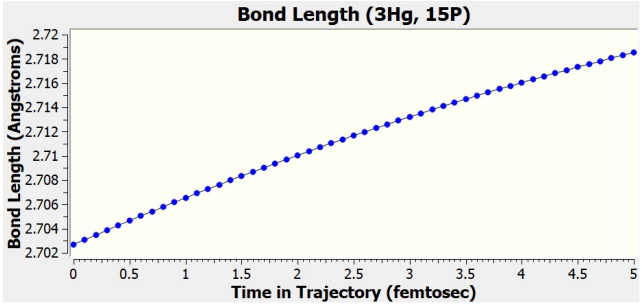
Bond Length (3Hg, 15P)
Bond Length (Angstroms)
2.72
2.718
2.716
2.714
2.712
2.71
2.708
2.706
2.704
2.702
0 0.5 1 1.5 2 2.5 3 3.5 4 4.5 5
Time in Trajectory (femtosec)

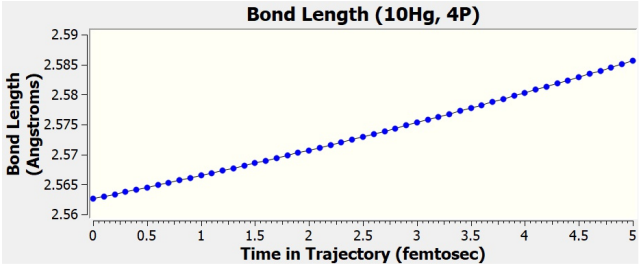
Bond Length (10Hg, 4P)
Bond Length (Angstroms)
2.59
2.585
2.58
2.575
2.57
2.565
2.56
0 0.5 1 1.5 2 2.5 3 3.5 4 4.5 5
Time in Trajectory (femtosec)

6s

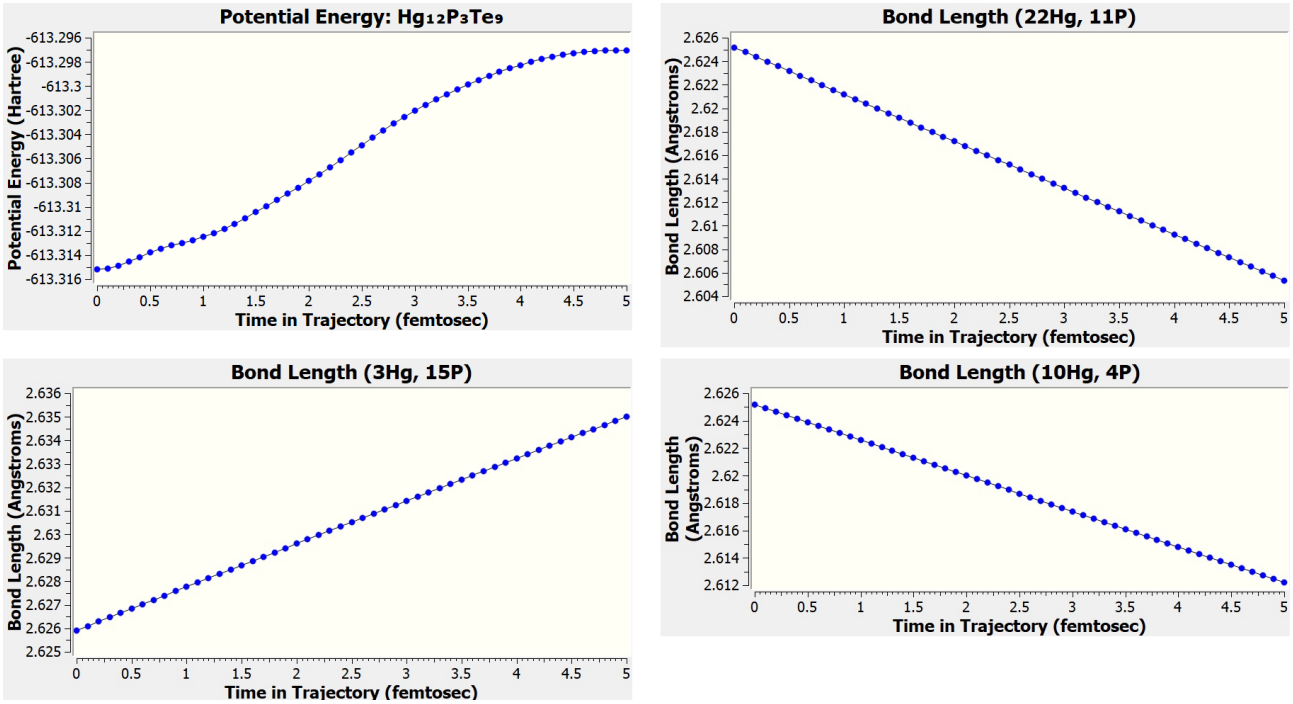

6t

Figure S6 (a–t): The ab initio molecular dynamics (AIMD) simulations were performed at an instantaneous temperature of 300 K (room temperature) to study the thermal stability of the system, i.e., how the potential energy and selected bond lengths (with neighboring atoms in the central honeycomb) change over a finite time (5 femtoseconds). As depicted, the changes in potential energy and bond lengths are very small and show smooth variations, with no sudden or abrupt fluctuations in energy or geometry. This indicates that the considered systems are thermally stable within the studied temperature range.

References

[1] Frisch, M. J., Trucks, G. W., Schlegel, H. B., Scuseria, G. E., Robb, M. A., Cheeseman, J. R., Scalmani, G., Barone, V., Petersson, G. A., Nakatsuji, H., et al. (2016). *Gaussian 09, Revision A.02*. Gaussian, Inc., Wallingford, CT.

[2] Franzke, Y. J., Bruder, F., Gillhuber, S., Holzer, C., Weigend, F. (2024). Paramagnetic nuclear /* magnetic resonance shifts for triplet systems and beyond with modern relativistic density functional methods. *The Journal of Physical Chemistry A*, **128**(3), 670–686.

[3] Jana, S., Patra, A., Constantin, L. A., Myneni, H., Samal, P. (2019). Long-range screened hybrid-functional theory satisfying the local-density linear response. *Physical Review A*, **99**(4).

[4] Peralta, J. E., Melo, J. I. (2010). Magnetic exchange couplings with range-separated hybrid density functionals. *Journal of Chemical Theory and Computation*, **6**(6), 1894–1899.

[5] Qu, Z., Liu, C. (2013). Intrinsic magnetism in edge-reconstructed zigzag graphene nanoribbons. In *Graphene Chemistry* (pp. 9–28). Wiley.

[6] Rivero, P., Moreira, I. de P. R., Scuseria, G. E., Illas, F. (2009). Description of magnetic interactions in strongly correlated solids via range-separated hybrid functionals. *Physical Review B*, **79**(24).

[7] Hay, P. J., Wadt, W. R. (1985). Ab initio effective core potentials for molecular calculations. Potentials for the transition metal atoms Sc to Hg. *The Journal of Chemical Physics*, **82**, 270–283.

[8] Chai, Jeng-Da, and Martin Head-Gordon. "Systematic optimization of long-range corrected hybrid density functionals." The Journal of chemical physics 128, no. 8 (2008).

[9] Gerber, Iann C., and János G. Angyán. "Hybrid functional with separated range." Chemical physics letters 415, no. 1-3 (2005): 100-105.

[10] Kumar, Vignesh Balaji, Szymon Smiga, and Ireneusz Grabowski. "A critical evaluation of the hybrid KS DFT functionals based on the KS exchange-correlation potentials." The Journal of Physical Chemistry Letters 15, no. 40 (2024): 10219-10229.

[11] Perilli, D., Chesnyak, V., Ugolotti, A., Panighel, M., Vigneri, S., Armillotta, F., Naderasli, P., *et al.* (2025). CO adsorption on a single-atom catalyst stably embedded in graphene. *Angewandte Chemie*, **137**(11), e202421757.

[12] Wella, S. A., Hamamoto, Y., Morikawa, Y., Hamada, I. (2019). Platinum single-atom adsorption on graphene: a density functional theory study. *Nanoscale Advances*, **1**(3), 1165–1174.

[13] Zuniga-Gutierrez, B., Camacho-Gonzalez, M., Simon-Bastida, P., Bendana-Castillo, A., Calaminici, P., Köster, A. M. (2015). Efficient calculation of the rotational g tensor from auxiliary density functional theory. *The Journal of Physical Chemistry A*, **119**(9), 1469–1477.

[14] Kita, Y., Tachikawa, M. (2009). Nuclear quantum effects on molecular magnetic properties. *Theochem*, **912**(1–3), 2–4.

[15] Yanai, T., Tew, D. P., Handy, N. C. (2004). A new hybrid exchange correlation functional using the Coulomb-attenuating method CAM-B3LYP. *Chemical Physics Letters*, **393**, 51–57.

[16] Elhorri, A. M. (2020). Theoretical study of new push–pull molecules based on transitioned metals for NLO applications and determination of ICT mechanisms by DFT calculations. *Journal of Theoretical and Computational Chemistry*, **19**(07), 2050026.

[17] Di Bella, S. (2010). Second-order nonlinear optical properties of transition metal complexes. *ChemInform*, **33**(13).

[18] Hatua, K., Nandi, P. K. (2013). Relationships between different-order polarizabilities and ground state dipole moment. *Journal of Theoretical and Computational Chemistry*, **12**(01), 1250099.

[19] Buckingham, A. D. (1967). Permanent and induced molecular moments and long-range intermolecular forces. In *Advances in Chemical Physics: Intermolecular Forces*; John Wiley & Sons, Inc., Vol. **12**, pp. 107–142.